Molecular determinants of cross-strain influenza A virus recognition by αβ T cell receptors

Sergio M. Quiñones-Parra[1#&], Stephanie Gras[2#$], Thi H.O. Nguyen[1], Carine Farenc[2], Christopher Szeto[2$], Louise C. Rowntree[1], Priyanka Chaurasia[2], Sneha Sant[1], Adrianus C.M. Boon[3], Dhilshan Jayasinghe[2$], Guus F. Rimmelzwaan[4], Jan Petersen[2], Peter C. Doherty[1], Adam P Uldrich[1], Dene R. Littler[2], Jamie Rossjohn[2,5*] and Katherine Kedzierska[1*]

[1]Department of Microbiology and Immunology, Peter Doherty Institute for Infection and Immunity, University of Melbourne, Parkville, Victoria, Australia.

[2]Infection and Immunity Program and Department of Biochemistry and Molecular Biology, Biomedicine Discovery Institute, Monash University, Clayton, Victoria, Australia.

[3]Department of Medicine, Washington University School of Medicine, USA.

[4]Research Center for Emerging Infections and Zoonoses, University of Veterinary Medicine, Hannover, Germany.

[5]Institute of Infection and Immunity, Cardiff University, School of Medicine, Heath Park, Cardiff UK.

[#]These authors contributed equally to this work.

Summary sentence: TCR-peptide-HLA ternary structures define molecular mechanisms of TCR cross-reactivity towards natural influenza variants.

*Joint senior and corresponding authors, K.K. (kkedz@unimelb.edu.au) and J.R. (jamie.rossjohn@monash.edu).

[&]Current address: Poseida Therapeutics, Inc. San Diego, CA.
[$]Current address: **Immunity & Infection Program,** La Trobe Institute for Molecular Science, Department of Biochemistry and Chemistry, La Trobe University, Melbourne, Victoria, Australia.

Running title: Broad cross-reactive TCR recognition of influenza epitopes

ABSTRACT

Cross-reactive αβ T cell receptors (TCRs) recognizing multiple peptide variants can provide effective control of rapidly evolving viruses yet remain understudied. By screening twelve naturally occurring influenza-derived HLA-B*35:01-restricted nucleoprotein $(NP)_{418-426}$ epitopes (B*35:01-NP_{418}), which emerged since 1918 within influenza A viruses, including 2024 A/H5N1 viruses, we identified functional broadly cross-reactive T cells universally recognizing NP_{418} variants. Binding studies demonstrated that TCR cross-reactivity was concomitant with diminished antigen sensitivity. Primary human B*35:01/$NP_{418}$$^{+}$$CD8^{+}$ T cell lines displayed reduced cross-reactivity in the absence of CD8 co-receptor binding, validating the low avidity of cross-reactive B*35:01-$NP_{418}$$^{+}$$CD8^{+}$ T cell responses. Six TCR-HLA-B*35:01/NP_{418} crystal structures showed how cross-reactive TCRs recognized multiple B*35:01/NP_{418} epitope variants. Specific TCR interactions were formed with invariant and conserved peptide-HLA features, thus remaining distal from highly varied positions of the NP_{418} epitope. Our study defines molecular mechanisms associated with extensive TCR cross-reactivity towards naturally occurring viral variants highly relevant to universal protective immunity against influenza.

INTRODUCTION

$CD8^+$ T cells play an important role in controlling respiratory viral infections, reducing disease duration, ameliorating disease outcomes and preventing life-threatening disease following seasonal, pandemic and avian influenza, respiratory syncytial virus (RSV) and COVID-19, as evidenced by studies in human cohorts (*1-7*) and animal models (*8-10*). Human influenza challenge of healthy volunteers showed that increased T cell cytotoxicity was associated with reduced virus shedding, even in the absence of antibodies (*1*). Similarly, prominent pools of influenza-specific memory T cells were associated with milder symptoms during the 2009 pandemic H1N1 infection (*2*) and against symptomatic PCR-confirmed influenza across several seasonal influenza epidemics (*3*). When the avian-derived influenza virus A/H7N9 emerged in China in 2013, causing mortality rates of >35%, patients with shortest hospital stays had cytotoxic $CD8^+$ T cell responses, whereas patients who had longer hospitalizations had delayed $CD8^+$ T cell immunity (*4*). In COVID-19, patients with prominent $CD8^+$ T cell responses towards an immunodominant $B7/N_{105}$ epitope had reduced viral replication and disease severity (*6*), while depletion of $CD8^+$ T cells in non-human primates abrogated protection against SARS-CoV-2 challenge (*11*). The importance of T cells in driving recovery from COVID-19 was also evident in immunosuppressed patients who lacked B cells, but recovered after inducing robust T cell responses (*12*). In both influenza virus infection (*10, 13, 14*) and RSV (*5*), resident memory $CD8^+$ T cells (T_{RMs}) within the respiratory tract are of particular importance for providing local immune responses, and controlling viral loads, disease severity and transmission (*10*).

$CD8^+$ T cells provide broadly cross-reactive immunity towards distinct influenza types and variants (*2, 4*) as well as SARS-CoV-2 variants of concern (VOCs) (*15, 16*), as they establish long-term memory pools directed towards epitopes (peptide (p) plus human leukocyte antigens (HLA)), encompassing predominantly conserved viral peptides (*17-19*). Thus, virus-specific $CD8^+$ T cell immunity, is a promising approach for broadly cross-reactive vaccines providing heterologous protective immunity across distinct strains and subtypes. If we can ameliorate disease severity from acute respiratory viral infections via establishment of prominent pre-existing T cell pools, we would be able to prevent life-threatening illness, especially in high-risk groups.

Nonetheless, the conservation of T cell-targeted viral peptides is not absolute, and influenza $CD8^+$ T cell escape occurs by several means, including abrogation of T cell receptor (TCR) recognition (*20*). $CD8^+$ T cell-mediated immune pressure can also drive emergence of influenza viral variants. A study in influenza virus-infected mice and an immunosuppressed individual with prolonged influenza disease revealed the emergence, persistence and

accumulation of naturally occurring variations within $CD8^+$ T cell epitopes over time, including the immunodominant $D^bNP_{366-374}$ epitope targeting influenza nucleoprotein (NP) (*21*). Importantly, in the absence of $CD8^+$ T cell-induced immune pressure (in major histocompatibility complex class I (MHC-I) irrelevant mice), viral variants can revert to the wild type viral peptide to restore viral fitness, demonstrating that the emergence and reversion of influenza virus quasispecies within $CD8^+$ T cell antigenic peptides can be driven by $CD8^+$ T cell immune pressure (*21*).

Eliciting TCRs, comprising of α and β chains ($\alpha\beta$ TCRs), capable of cross-reacting with a broad array of naturally occurring viral-peptide variants could circumvent $CD8^+$ T cell immune escape and yield a highly sought measure of universal protective immunity against influenza. Although the TCR repertoire is theoretically smaller than the number of potential antigens presented by HLA molecules, the coverage of foreign antigens can be achieved by a degree of TCR cross-reactivity, as shown in autoimmunity (*22, 23*), cancer (*24*), and towards the human telomerase reverse transcriptase (*25*). Cross-reactivity of TCRs, in which $CD8^+$ T cells can respond to different peptide-HLA complexes, is of fundamental importance for our understanding of T cell immunity and has relevant implications for broadly protective immunity in infection and cancer (*3*). However, to date, molecular determinants of broad cross-strain recognition of naturally emerging viral variants by $\alpha\beta$ TCRs remain unclear.

Our study defines molecular mechanisms of TCR cross-reactivity towards naturally occurring viral variants by αβ TCRs, focusing on natural influenza variants within the HLA-B*35:01-restricted $NP_{418-426}$ (B*35:01-NP_{418}) epitope (*26*), including 2024 avian and bovine H5N1 viruses. The cross-reactive capacity of $CD8^+$ T cells directed at B35/NP_{418} variants was previously reported at polyclonal and clonal levels, and suggested to be driven by prior infections with distinct influenza viruses that selected cross-reactive $CD8^+$ T cells reactive to B*35:01-NP_{418} variants (*26, 27*). We analyzed HLA-B*35:01/B*35:03/B*07:02 $CD8^+$ T cell responses across twelve $NP_{418-426}$ naturally-occurring variants in healthy participants and patients undergoing pandemic (p)H1N1 2009 influenza virus infection, revealing a larger extent of $CD8^+$ T cell cross-reactivity towards this epitope (*20*). Influenza-specific memory $CD8^+$ T cells from healthy participants were reactive to 10 out of 12 NP_{418} variants and up to 11 in pH1N1 2009 infected patients (*20*). Thermal stability assays and structures of HLA-B*35:01 in complex with six NP_{418} peptides determined that these complexes were stable and contain solvent exposed amino acids at p4 and p5 in NP_{418} that resemble potential TCR contacts (*20*). This antigenic peptide variability along with the spectrum of clonal $CD8^+$ T cell cross-reactivity, make the HLA-B*35:01-NP_{418} epitope valuable for interrogating molecular

determinants of specificity and cross-reactivity of influenza-specific TCRs, highly relevant to other viral infections.

Here, we generated and studied six ternary TCR-NP_{418}-HLA-B35 structures to unravel molecular determinants of TCR recognition of naturally emerging viral variants within one of the most immunodominant human $CD8^+$ T cell epitopes reported to date, B35/NP_{418}. Our question was to understand why some B35/NP_{418}-specific TCRs are more specific (or narrow) in recognition, while other TCRs display broader recognition in the context of natural T cell variable antigens. In human primary B*35:01/NP_{418} $^+CD8^+$ T cell lines, we further verified low avidity of cross-reactive B*35:01/$NP_{418}^+CD8^+$ T cell responses by showing markedly reduced cross-reactivity in the absence of CD8$\alpha\beta$ co-receptor binding. We identified a large spectrum of heterogeneous HLA-B*35:01-NP_{418} cross-reactive $CD8^+$ T cell pools, both at the polyclonal and clonal levels. Polyclonal, cross-reactive HLA-B*35:01-$NP_{418}^+CD8^+$ T cells clustered around NP_{418} variants sharing D and K/R residues at solvent-exposed p4 and p5, respectively. TCR affinity was negatively associated with the breadth of TCR cross-reactivity. NP_{418} variants recognized with lower avidity were nonetheless capable of eliciting multiple effector functions. Structural studies showed that the cross-reactive TCRs were mainly recognizing the epitope via backbone contacts, alongside permissive interactions with charged p4/p5 residues. Notably, cross-reactive TCRs remained distant from the hypervariable residues of the NP_{418} epitope. Accordingly, we provide a molecular understanding of how TCR cross-reactivity towards a variable influenza epitope is manifested, highly relevant to understanding universal protective immunity against influenza and potentially other viral diseases.

RESULTS

Broad cross-reactivity of influenza-specific CD8$^+$ T cells directed against HLA-B*35:01/NP$_{418}$ variants

An influenza-derived NP$_{418-426}$ epitope is an immunodominant human CD8$^+$ T cell target (*20, 21, 28*), presented by at least 3 HLA allomorphs of the highly prevalent HLA-B7 superfamily (*29*), HLA-B*07:02, HLA-B*35:01 and HLA-B*35:03. Although >20 NP$_{418}$ variants have been found within influenza A viruses circulating over the last century, including avian and bovine 2024 H5N1 viruses, B35*01/NP$_{418}$-specific CD8$^+$ T cells display a high degree of cross-reactivity towards different NP$_{418}$ variants (*20, 21, 28, 30*). To understand the plasticity of B35*01/NP$_{418}$-specific CD8$^+$ T cells in recognizing a selected array of variants, we focused our analyses on 10-12 of NP$_{418}$ variants that cover all the major human and avian influenza viruses (Table 1, Fig. 1A).

To study B*35:01-NP$_{418}$-specific CD8$^+$ T cells, we generated HLA-B*35:01-tetramers loaded with 10 different naturally-occurring NP$_{418}$ peptides (Fig.1A, fig. S1) and stained polyclonal HLA-B*35:01/NP$_{418}$-specific cells expanded *in vitro* (Fig. 1B). At 11 days (d) after peptide stimulation, HLA-B*35:01/NP$_{418}$ CD8$^+$ T cells were detected in 3 out of 4 donors with frequencies ranging from ~1-25% of CD8$^+$ T cells (Fig. 1C), whereas one donor had negligible tetramer$^+$ events above background staining. Variations in the frequencies of B*35:01/NP$_{418}$ tetramer$^+$ CD8$^+$ T cells were donor-dependant and NP$_{418}$ variant-dependant, likely reflecting the individual's influenza history (*13*). To determine cross-reactivity within HLA-B*35:01-NP$_{418}$ CD8$^+$ T cells, we co-stained with a tetramer matrix covering the plausible unique HLA-B*35:01-NP$_{418}$ tetramer combinations (Fig. 1D, fig. S2). Streptavidin to monomer conjugation ratios were optimized using BaF3 cells expressing the β2M agonist LILRB1, whereby free monomer-streptavidin 'cross-over' during tetramer co-staining was excluded (fig. S1). Cross-reactivity towards HLA-B*35:01-NP$_{418}$ was heterogeneous, however, larger pools of cross-reactive cells clustered around NP4, NP5 and NP6 variants (Fig. 1E & F), exposing the DKS/DKT sequence that is solvent-exposed and in the central P4, P5, and P6 epitope positions (Fig. 1A). The middle part of the epitope is preferred for TCR interactions. These results show that polyclonal populations of cross-reactive memory HLA-B*35:01/NP$_{418}$-specific CD8$^+$ T cells are present in the majority of HLA-B*35:01$^+$ individuals, resolving a large extent of mostly heterogeneous cross-reactivity directed against a hypervariable influenza CD8$^+$ T cell epitope.

HLA-B*35:01/NP_{418}-specific cross-reactivity at a single TCR level

To cover the spectrum of cross-reactive responses towards HLA-B*35:01/NP_{418} variants by single TCR$\alpha\beta$, we selected four primary HLA-B*35:01/$NP_{418}^{+}CD8^{+}$ T cell clones, derived from 2 HLA-B*35:01^{+} donors, recognizing 1 or 4 (out of 4 variants tested) $NP_{418\text{-}426}$ variants (*21, 31*). Using single-cell paired TCRαβ RT-PCR sequencing, Complementary Determining Region (CDR) TCR clonotypes were defined and their clonality was confirmed (Table 2). To dissect TCR specificity for HLA-B*35:01/NP_{418} variants in a controlled system, we transiently expressed CD3, TCR and CD8αβ molecules in HEK293T cells and performed HLA-B*35:01/NP_{418} tetramer binding analysis (fig. S3). These HLA-B*35:01/$NP_{418}^{+}CD8^{+}$ T cell clones expressed distinct TRAV- and TRBV-chains except for a TRBV20-1*01 chain shared between TCR.2384 and TCR.3180, however with different TRBJ segments (Table 2). Despite the relative diverse V gene usage and CDR3 sequences, TCRαβ clones shared common characteristics, including shared TRBJ chain usage of TCR.D1 and TCR.2384 and, consequently, a common QETQ motif within CDR3 (Table 2). Moreover, the TCR.C4 and TCR.3180 clones displaying a greater degree of cross-reactivity, shared a G and a QL motif in CDR3α, and a P in the CDR3β (Table 2).

To investigate the functional consequences of TCR-mediated cross-reactivity across 12 naturally-occurring variants of HLA-B*35:01/NP_{418}, covering the major human and avian IAVs, we transduced Jurkat76 (J76) cells with TCR segments corresponding to clones D1, 2384, C4 and 3180. We measured activation mediated by these HLA-B*35:01/NP_{418}-specific TCRs towards 12 different NP_{418} peptides (or the pool of 12 NP_{418} peptides as a control) by CD69 surface expression. The NP_{418} peptide pool induced TCR-specific activation and CD69 upregulation on $CD8^{+}CD3^{+}GFP^{+}$, HLA-B*35:01-NP_{418}-specific J76 cells (Fig. 2A & B), but not for HLA-B*07:02-expressing cells (Fig. 2B), confirming TCR specificity and self-HLA restriction at the functional level.

The extended analysis with single-peptide stimulations revealed the breadth and profiles of clonal cross-reactivity of HLA-B*35:01/NP_{418}-specific TCRs (Fig. 2C & D). The NP_{418} variants NP4, NP6 and NP8, bearing a DKS/DKA motif were broadly recognized by the four TCRs (Fig. 2C & D). We observed that the NP_{418} variants NP1, NP2, NP9, NP11 and NP12 containing a R or I at p5, induced negligible (NP1, NP2 and NP12) to no (NP9 and NP11) functional activation across the four TCRs analysed (Fig. 2C & D). Moreover, a substitution of a positively-charged polar residue to a smaller hydrophobic side-chain, K→I also at p5 in NP9

(LPF**DIA**T**I**M), likely impacted the pHLA surface available for TCR contact (*20*) and did not induce CD69 upregulation in any of the B*35:01/NP_{418}-specific J76 lines (Fig. 2C & D). TCR3180 displayed the largest breadth of recognition of 9 NP_{418} peptide variants out of 12, while TCR.C4 displayed the second largest breadth of recognition with 7 NP_{418} peptide variants out of 12. All variants recognized by TCR.C4 had D at P4 and either a R or a K at p5, and it was the only TCR not recognizing NP7 (LPF**EKS**T**I**M) (Fig. 2C & D).

Accordingly, we demonstrate that the breadth of cross-recognition of HLA-B*35:01-NP_{418}-reactive TCRs ranges between 5 and 9 out of 12 NP_{418} variants and revealed shared and unique cross-reactive profiles, most likely driven by their TCR$\alpha\beta$ characteristics.

Functional avidity and affinity of TCR-HLA-B*35:01-NP_{418} interactions

To address whether the breadth of cross-reactivity impacted the functional T cell avidity, we performed kinetic peptide-dose response experiments for the peptides recognized by TCRs D1, 2384, C4 and 3180 (Fig. 3A). These saturation curves allowed us to calculate half maximum effective concentrations (EC_{50}) values, reflective of antigen sensitivity (Fig. 3B). Moreover, Surface Plasmon Resonance (SPR) assays assessed the affinity of the NP-variants (all but NP11) for D1 and 3180 TCRs (table S1).

TCR.D1-expressing cells recognized NP_{418} variants with two largely different antigen sensitivities, NP6, NP7 and NP10 (LPF**DKS**T**V**M, LPF**EKS**T**I**M and LPF**EKS**T**V**M respectively), all of them sharing p5-K, p6-S present an EC_{50} of ~$10^{-9.3}$ LogM (Fig. 3A & B). Affinity was determined via SPR to be >200 μM, ~110μM and ~40 μM, respectively (table S1). Conversely, the EC_{50} was reduced by ~1.8 LogM for variants with the V-I substitution at p8 (NP8, LPF**DKA**ST**I**M and NP4-LPF**DKS**T**I**M) (Fig. 3A & B), and we could not observe binding via SPR (table S1). Interestingly, the only difference between NP10 and NP7 peptide is the V→I substitution at p8. This substitution did not influence the EC_{50} but reduced the binding affinity from ~40 μM (NP10) to ~ 110μM (NP7). This indicates that p8 plays a role in antigen recognition, suggesting that the extensive drift observed at this position could be $CD8^+$ T cell-mediated (Table 2). The antigen sensitivity profile of TCR.2384 showed highest functional avidity for NP4 (LPF**DKS**T**I**M) (EC_{50}~$10^{-8.7}$ LogM), followed by NP5 and NP8 (LPF**DKT**T**I**M and LPF**DKA**T**I**M) with an EC_{50}~$10^{-7.5}$ LogM, exposing a preferred **DKx/I** (residues p4 p5/p7) motif (Fig. 3A & B).

TCR.C4 was most sensitive, with an EC_{50} $<10^{-7.5}$ LogM, towards the NP3, NP4 and NP6 peptides (LPF**DKP**T**I**M, LPF**DKS**T**I**M and LPF**DKS**T**V**M, respectively), and antigen sensitivity was somewhat marginally reduced by 0.4 LogM for NP5, LPF**DKT**T**I**M and NP8, LPF**DKA**T**I**M (Fig. 3A & B). Except for antigen sensitivity towards NP2, LPF**DRT**ST**I**M (EC_{50}~$10^{-6.5}$LogM), the most cross-reactive TCR.3180 recognized 8 of the NP_{418} variants with similar pHLA-I avidities (EC_{50} range=$10^{-7.1}$-$10^{-8.6}$LogM) (Fig. 3A & B) and 7 of these peptides displayed K at p5 (Fig. 3A & B). Thus, consistent with its broadest cross-reactivity (breadth=9 variants out of 12), the preferred peptide motif was **xKx/x**. Similar observations were made with the SPR experiments that showed 2 different populations according to binding affinity: NP4, NP5, NP7 and NP8 with affinities around 10 – 15 μM, and NP3, NP6, NP10 and NP12 with affinities from ~40 to 100 μM (Table S1). No binding was observed for NP2, which also had the lowest EC_{50} (Fig. 3B).

Functional avidity correlated with TCR affinity, determined by SPR assays, further validating the utility of antigen sensitivity as a measure of the strength TCR-HLA-B*35:01-NP_{418} interactions. Collectively, we revealed the interplay between TCR specificity and pHLA-I avidity. TCRs D1 and 2384 displayed higher specificity, recognizing less peptide variants with large differences (of up to 10^{-2}LogM in EC_{50}) in TCR-HLA-B*35:01-NP_{418} avidity antigen sensitivity (Fig. 3B). Conversely, the less specific TCR.C4 and TCR.3180, recognized more NP_{418} variants, albeit with lower functional pHLA-I avidities (Fig. 3B). Thus, higher TCRαβ cross-reactivity comes at the expense of compromising HLA-B*35:01/NP_{418} avidity.

CD8β co-receptor binding dependence of cross-reactive HLA-B*35:01-$NP_{418}$$^{+}$CD8^{+} T cell responses

As CD8β co-receptor binding dependence is a hallmark of low avidity influenza-specific CD8^{+} T cells (*32-34*), we generated 7 HLA-B*35:01/NP_{418} CD8-null monomers, containing Q226K and D227A mutations within HLA-B*35:01 to abrogate CD8β binding (table S2) to validate reduced avidity of cross-reactive HLA-B*35:01-$NP_{418}$$^{+}$CD8^{+} T cell responses. Primary human HLA-B*35:01-$NP_{418}$$^{+}$CD8^{+} T cell lines on d11 following stimulations with NP_{418} peptide pools were co-stained with the wild type and CD8-null HLA-B*35:01/NP_{418} tetramers, conjugated to different fluorochromes (Fig. 4, fig. S4). Our data showed that the primary human B*35:01/$NP_{418}$$^{+}$CD8^{+} T cell lines displayed markedly reduced cross-reactivity in the absence of CD8β co-receptor binding, confirming our findings in NP_{418} Jurkat cells of low avidity of cross-reactive B*35:01/$NP_{418}$$^{+}$CD8^{+} T cell responses.

Mutational analysis of NP_{418} and requirements for TCR activation

To identify the key sites for TCR activation, we performed alanine substitution scans using the broadly recognized NP4 epitope as proxy (Fig. 5A-D). A was substituted into positions P1, P4, P5, P6, P7 or P8, while the remaining P2, P3 and P9 positions were kept unaltered due to their roles in peptide anchoring to HLA-B*35:01 (*20*) (Fig. 5E).

TCR.3180 displayed the highest degree of tolerance to mutations in NP4 consistent with its broadly cross-reactive profile (Fig. 5D). Nevertheless, A at the invariant p7-T and at p8-I resulted in an 80% decrease in T cell activation (Fig. 5D). Despite TCR.D1 being at the lower end of cross-reactive capacity (5 NP_{418} variants recognized Vs 7 by TCR.C4 and 9 by TCR.3180), this clonotype tolerated 4 out of 6 A substitutions in the peptide (Fig. 5A). TCR.D1 clonotype activation was only disrupted by mutations in the pivotal p5 or p7 positions (Fig. 5A & B). Interestingly, A-substitutions at P4 resulted in ~50% increase in CD69 expression relative to wild-type NP4, revealing a unique feature of this TCR (Fig. 5A). TCR.D1 activation was altered following stimulation with A substitutions at P1, P5, P7 and P8 relative to wild type NP4 (Fig. 5A).

TCR.2384 failed to upregulate CD69 expression when p5, p7 and p8 were altered and TCR activation decreased by ~70% with the A4 mutation in NP4 (Fig. 5B). Overall, TCR.2384 required integrity of the central (p4 and p5) and C-terminal residues (p7 and p8) (Fig. 5B). Thus, despite TCR.2384 sharing clonotypic and specificity features with TCR.D1 (Table 2 & Fig. 2C & D, Fig. 3A & B), it displayed distinct requirements along the NP4 peptide sequence for activation. TCR.C4 had a breadth of recognition of 7 peptide variants (Fig. 2C & D, 3A & B), however, only 2 out 6 altered peptide ligands were recognized, representing the lowest (out of four TCRs analysed) tolerance for alterations in the NP4 peptide (Fig. 5C).

Overall, these experiments indicate that p5 acts as a major pivot for NP_{418} TCR recognition. The specific requirements in the peptide sequence for T cell activation suggest distinct modes of TCR-HLA-B*35:01-NP_{418} recognition. These data indicate that cross-reactivity towards HLA-B*35:01/NP_{418} is, to an extent, driven by plasticity in cross-reactive TCRs.

Cytokine and polyfunctional profiles of primary HLA-B*35:01/NP_{418}-specific $CD8^+$ T cell clones

To define functionality of HLA-B*35:01/NP_{418}-specific $CD8^+$ T cell clones, we determined cytokine-producing profiles of primary T-cell clones to different NP variants displayed on C1R

cells. We performed intracellular cytokine staining (ICS) by stimulating primary D1 and 3180 clones with a panel of NP peptide-pulsed HLA-B*35:01$^+$ C1R cells. Negative controls included HLA-B*35:01$^+$ C1R cells pulsed with nil or HLA-matched but irrelevant IPS peptide. Controls included primary T-cell clones stimulated with HLA-B*35:01$^+$ C1R cells pulsed with NP peptide-pool, PMA/Ionomycin or anti-CD3/anti-CD28 beads.

Clone D1 produced highest levels of IFN-γ production (>75%) following exposure to NP6, NP7 and NP10, while Clone 3180 responded highest to NP4, NP5, NP7, NP8 and NP10 (Fig. 6A), reflective of their antigen sensitivity patterns (Fig. 3). Multifunctional T cell activation profiles comprising cytokines IFN-γ, TNF-α and MIP-1β and degranulation marker CD107a (Fig. 6B) showed similar activation patterns with clone D1 showing highest polyfunctionality towards NP6, NP7 and NP10, and clone 3180 towards NP4, NP5, NP7, NP8 and NP10 (Fig. 6C). Therefore, the primary T cell clone's cytokine profiles functionally confirm their antigen recognition patterns towards NP variants.

Similar conformation of NP_{418} variants in the HLA-B*35:01 binding cleft

To gain insights into the nature of NP_{418} variants, we determined high-resolution structures of HLA-B*35:01 presenting five NP_{418} peptides: NP3, NP6, NP7, NP8 and NP9 (fig. S5 and table S3). Epitope variants adopt a similar conformation in the HLA-B*35:01 binding cleft, with an average root mean squared deviation (r.m.s.d.) of 0.24 Å^2 when compared with the NP_{418}/HLA-B*35:01 structure as reference (pdb: 3LKS). The P2-P and P9-M anchor residues, lie deep within the peptide-binding groove positioning the central portion of the epitope for outward display (Fig. 5E, fig. S5A-D). At the N-terminal end the peptide backbone undergoes near right-angle transitions at both the P3-F and negatively charged P4 yielding a distinctive kink to this HLA-presented epitope following the P2-P anchor (fig. S5A). The divergent residues present in individual viral strains project upward from HLA-B*35:01 at positions P4, P5, P6 and P8. The charged P5 residue provides a prominent extension and is somewhat mobile about its alkyl chain.

Alternate mechanisms of D1 and 3180 TCRs for cross-reactivity

To understand T cell cross recognition, we determined the structures of the cross-reactive 3180 TCR (TRAV13-1, TRBV20-1*02) in complex with HLA-B*35:01 presenting NP4, NP7 and NP8 and the D1 TCR (TRAV1*01, TRBV7-8*01) in complex with HLA-B*35:01 presenting NP6, NP7 and NP10 (Fig. 7, fig. S6 and tables S4-S7). A comparison of three 3180 TCR HLA-B*35:01/NP variant structures showed that docking angles, total buried surface area (BSA) and individual CDR contributions were essentially unchanged (all TCR Cα r.m.s.d. = 0.37 -

0.51 Å), which was also the case for the three D1 TCR HLA-B*35:01/NP complexes (TCR Cα r.m.s.d. = 0.37 - 0.81 Å). To enable a detailed comparison, we analysed complexes formed between the HLA-B*35:01-NP7 epitope and TCRs 3180 and D1. Overall, HLA-B*35:01-NP7 was engaged by the 3180 and D1 TCR with a similar, canonical docking mode, crossing the central portion of the peptide at an angle of 63˚ and 77˚, respectively (table S5). In line with disparate CDR3 loop sequences and TRAV/TRBV gene usage (table 2), the fine positioning of 3180 and D1 TCRs relative to HLA-B*35:01/NP, and the layout of CDR loops was overall distinct (TCR Cα r.m.s.d. = 3.5-3.6 Å), and there were few, if any, conserved features in pHLA-B*35:01 recognition (Fig.7 and fig. S6).

Structure of the 3180 TCR HLA-B*35:01-NP7 complex

The complex formed between the 3180 TCR and HLA-B*35:01-NP7 comprised a total BSA of 2040 $Å^2$ with TCRα and TCRβ chains contributing roughly equal shares to the total BSA (47.8% and 52.2 %, respectively) (tables S5-S7). The interface was dominated by CDR3β (BSA: 34%), which occupied a central position atop of the peptide and interacted with both sides of the peptide binding groove, via T69 and T73 on the HLA α1-helix and A150, R151 and Q155 on the α2-helix (table S7). The remaining CDR loops occupied peripheral positions and provided sizeable interface with the HLA that neatly encased the central CDR3β (fig. S6A & C). Residues CDR3β 108 – 112 were aligned alongside the NP7 peptide, forming five H-bonds (p5-K, p6-S and p7-T), two salt bridges (p4-E and p5-K), and numerous van der Waals (vdW) interactions across p5-p7 of the peptide (fig. 7C and table S4). In addition, CDR3α D107 contributed a single salt bridge interaction with p5-K, while CDR1α contributed vdW interactions with p8-I (table S5). Accordingly, TCR 3180 - peptide interactions were almost exclusively mediated by the TCR β-chain.

Structural basis for 3180 TCR - NP variant cross-reactivity

The structures of 3180 TCR-HLA-B*35:01/NP_{418} epitope variant complexes revealed several features that underpin 3180 TCR tolerance to epitope variation. Specifically, T cell activation assays demonstrated that the 3180 TCR retains reactivity to variant epitopes carrying conservative substitutions in p4 (D, E), p5 (K>R), p6 (S, A > T, P) and p8 (I>V) (Fig. 2). Compared to the unbound epitope structures that displayed some conformational variability in p4-p8 of the NP epitope variants, 3180 TCR binding imposed a single conformation upon each peptide as it was entombed between the HLA platform and TCR CDR loops (fig. S5B and S6E). Presumably, this induced fit feature confers a degree of tolerance to conformational diversity and variable flexibility of peptide residues. Further, the 3180 TCR

provides opposing charges for the charged p4 and p5 residues (p4-E and p5-K in NP7), and, notably, 3 H-bond interactions to the p5-K sidechain (Fig. 7C, table S7). Accordingly, tolerance of conservative substitutions in p4 and p5 is enabled by electrostatic complementarity between CDR3 residues and the peptide. Furthermore, the extended alignment of the CDR3β backbone with the peptide confers three β-sheet-like backbone-backbone H-bonds between CDR3β T109, S110 and R112 and the backbone of variable peptide residues p4, p5 and p6 (Fig. 7C), which likely contributes to sidechain substitutions in the central portion of the peptide.

The TCR.C4 and TCR.3180 clones, that display a greater degree of cross-reactivity, shared a YQL114-116 motif in CDR3α unique to the TRAJ33 and TRAJ28 segments used by TCR.C4 and TCR.3180, respectively, as well as P108 in CDR3β (Table 2). While it remains unclear how far these features contribute to cross-reactivity, CDR3α Y114 plays a structural role in the TCR 3180 - HLA-B*35:01 interface, where it interconnects the tip of CDR3β (G111, R112) with HLA-B*35:01 α1 helix residues Q65 and I66 (Fig. 7C, fig. S6A and table S7), whereas CDR3β P108 is responsible for a kink in the CDR3β backbone that aligns CDR3β108-112 alongside the peptide, and enables aforementioned H-bonding with the peptide backbone.

Structure of the D1 TCR HLA-B*35:01-NP7 complex

Broadly comparable to the 3180 ternary complex, the interface of the D1 TCR and HLA-B*35:01 NP7 complex was similar footprint with a total BSA of 2000 Å^2, TCRα and TCRβ BSA contributions were evenly matched, with 47.6% and 52.4 %, respectively, and the CDR3β loop made the largest BSA individual contribution (22.9%) (Fig. 7D-F, fig. S5D, S6B & S6F). As observed in the 3180 TCR B*35:01 NP7 complex, CDR3β took up a central position atop of the peptide, with the CDR3β$^{119\text{-}113}$ backbone of partially aligned along the peptide. CDR3β formed an expansive interface with the peptide, including 5 hydrogen bonds and multiple van der Waals interactions across p3 to p8 of the peptide and a smaller interface with the B*35:01 α2 helix. In analogy to 3180 (Fig. 7B & C), the peptide interface of the D1 TCR was expansive and dominated by CDR3β, and it involved multiple interactions with the peptide backbone (p4, p5, p7 and p8). D1 TCR peptide interactions included three hydrogen bonds between CDR1α Y37, CDR3α G113, CDR3β T109 and the backbone of p4-E (2 hydrogen bonds) and p8-I, as well as two H-bonds between CDR3β G112Q113 and the p5-K sidechain (Fig. 7E & F). Accordingly, the interface between the D1 TCR and HLA-B*35:01 NP7 was altogether distinct from that of the 3180 TCR, in that it employed different residues and a less polar bonding pattern, but it also reiterated elements of the 3180 TCR interface that was heavily

involved with the peptide backbone and formed focal H bonds with the p5-K sidechain (Fig. 7E & F). As observed in the 3180 ternary complexes, the D1 TCR locked each peptide variant into a fixed position, with the distinction that the sidechain of p5-K assumed a distinct conformation (fig. S6F), attributable to H-bonding between the p5-K sidechain and HLA-B*35:01 α2 helix residues A150 and Q155.

Structural basis for D1 TCR - NP variant cross reactivity

We examined how the D1 TCR accommodated epitope variations. This TCR forms three hydrogen bonds between its CDR loops and the peptide backbone and 2 more with the NP7 P5-K sidechain. The peptide backbone interactions such as that made by ^{D1}CDR1α Y37 obviously permit significant variant substitutions (Fig. 7F) as would the van der Waals with the p7-T (Fig. 7F) and the backbone-backbone interactions to P8 (Fig. 7F). Specific features of the P4 side chain remain distal from the TCR, a van der Waals contact is made to Cβ carbon potentially allowing multiple substitutions at this site. In contrast, the positively charged p5 extends to become sandwiched between ^{D1}CDR3β and the HLA α1 helix via multiple H-bonds (fig. S6D). This key interaction is thus less permissive than the equivalent salt-bridge of the 3180 TCR limiting the D1-TCR's tolerance of substitutions at this position (Fig. 2). The highly variable p6 and p8 positions are also far more buried in the D1 complex as compared to that of 3180 but their side chains remain surrounded by water-filled cavities allowing for limited substitution at these sites.

The major contributor to NP epitope binding in both the 3180 and D1 TCR, is the CDR3β loop. A commonality achieved as both cross-reactive TCRs bind to the varied influenza epitopes via direct interactions to conserved features (*e.g.* p3 and p7) yet utilize more accommodating interactions to varied epitope positions (*e.g.* p4 and p5). An outcome accomplished in fundamentally distinct ways for each cross-reactive TCR.

DISCUSSION

The importance of antigen-specific CD8$^+$ T-cell memory for protection against severe influenza disease caused by seasonal and newly-emerging viruses in the absence of pre-existing antibodies has been reported (*1, 35*). Our study defines a highly immunodominant and cross-reactive influenza-specific CD8$^+$ T cell response in HLA-B*35:01$^+$ individuals that can recognize up to 9 out of 12 influenza A NP_{418} variants spanning over 100 years, including the currently circulating avian and bovine 2024 H5N1 viruses. While a high proportion of

influenza-specific $CD8^+$ T cell epitopes is conserved (*17*), variability in T cell viral targets occurs naturally (*20*) (*21*). The B35/NP_{418} epitope represents one of the most variable immunodominant influenza $CD8^+$ T cell epitope. It is currently also the most cross-reactive influenza $CD8^+$ T cell response across viral variants, particularly to a region of high diversity within influenza A nucleoprotein. Our study defines molecular mechanisms of cross-strain influenza A virus recognition by αβ TCRs directed towards epitopes encompassing a highly diverse range of naturally occurring viral variants. To the best of our knowledge, no other study has undertaken this level of depth and detail towards unravelling molecular determinants of TCR cross-recognition towards multiple naturally occurring viral variants for such an extensively studied diverse immunodominant $CD8^+$ T cell epitope. Prior work investigated immunity to hypervariable epitopes in autoimmunity (*22*), cancer (*24*) and towards the human telomerase reverse transcriptase (*25*). B35/NP_{418}-specific epitopes studied here are relevant in a natural context of influenza viral mutations, providing real-life relevant evidence on T cell cross-reactivity. Our work also provides insights into epitope-specific $CD8^+$ T cell responses to naturally emerging variants in other viral infections. It is important to note that while early antigen-specific $CD8^+$ T cells ameliorate disease severity (*4*), bystander and/or late (*36, 37*) $CD8^+$ T cell responses can contribute to lung injury (*38*).

Our question was to understand mechanisms why some B35/NP_{418}-specific TCRs are more specific (or narrow) in recognition, while other TCRs display broader recognition in the context of natural T cell variable antigens. To define TCR cross-strain recognition of influenza A viruses, we established a TCR expression system in J76 cells to analyze functional consequences of TCR binding to distinct influenza antigenic peptides (natural or altered) presented by HLA-B*35:01. We revealed an unanticipated breadth of TCR recognition of multiple influenza pHLA variants. We propose that this cross-recognition is mediated by the interplay between the TCRs ability to tolerate substitutions in the antigenic peptide, while maintaining pHLA avidity at levels that are sufficient to drive TCR activation. These findings were validated in our primary human HLA-B*35:01-$NP_{418}{}^+CD8^+$ T cell lines stimulated with NP_{418} peptide pools, then co-stained with single wild type and CD8-null HLA-B*35:01/NP_{418} tetramers to assess cross-reactivity. Our data clearly revealed markedly reduced cross-reactivity in the absence of CD8β co-receptor binding, confirming our findings in NP_{418} Jurkat cells of low avidity of cross-reactive B*35:01/$NP_{418}{}^+CD8^+$ T cell responses. These findings were supported by TCR-B*35:01/NP_{418} affinity measurements.

Different molecular mechanisms allow the cross-reactive D1 and 3180 TCRs to each interact with a broad array of epitopes, doing so by remaining distal form hyper-mutable residues, forming specific-interactions to invariant residues and permissive contacts to

strain-variant residues. $NP_{418-426}$ is one of the most heavily targeted influenza T cell antigenic regions as it is promiscuously presented by multiple HLAs and is known presently to be restricted by HLA-B*35:01 (*27*), HLA-B*35:03 (*20*) and HLA-B*07:02 (*39*)) of the B7 supertype (*40*). These HLAs are highly prevalent, to an extent that in some ethnically diverse populations they can be among the most frequently used (*39*). The variational change in NP_{418} has not been documented for other influenza $CD8^+$ T cell antigenic peptides, making it surprisingly diverse for an immunodominant acute-viral epitope.

The D1 and 3180 TCRs recognize multiple NP_{418} variants in different ways. The 3180 TCR binding to HLA-B*35:01-NP is a focused epitope-CDR3β β-sheet-like alignment that facilitates positioning of permissive electrostatic interactions near the charged yet changeable p4 and p5 positions. A β-sheet-like recognition system is ideal for a cross-reactive TCR as it is essentially indirectly "reading" the epitope's inter-anchor backbone conformation. NP_{418}-HLA-B*35:01 structures imply that the NP_{418} backbone structure is tolerant of considerable substitution, thus potentially explaining the broad cross-reactive profile of 3180 TCR. At the start of the β-sheet-like alignment, the interaction with the p7-T is integral to the 3180-NP-HLA-B*35:01 binding mechanism, any p7 substitution other than serine should compromise recognition confirmed in our epitope alanine scanning experiments. We note that this p7 residue, T424, is highly conserved across sequenced human influenza viruses.

The electrostatic pockets of the ^{3180}CDR3β include a R112 interaction that equally accepts an epitope p4-D or p4-E. In the 3180 TCR co-complex structures, the epitope's p5-K extends to form a salt-bridge within an electrostatic pocket, also able to accommodate NP12's p5-R, albeit at some cost to activation potential. The J76 activation experiments were consistent with the fact the 3180 TCR avoided all contact with the hypervariable P6 and P8 side chains. The D1 TCR forms a fundamentally distinct set of contacts to the NP_{418} epitope, like 3180 several interactions are made directly to critical points in the backbone structure, including numerous CDR-epitope backbone interactions. However, these arise from residues in multiple CDR loops and from both TCR chains. Unlike 3180, whose interactions stem primarily from a single CDR loop, the D1 TCR overlays the NP_{418} more completely, yet it leaves significant space near the hypervariable p6 and p8 positions. Its binding mechanism is also highly focused around the p5-K, but instead of forming a high-affinity distance-tolerant salt-bridge, a cluster of H-bond contacts is contributed by ^{D1}CDR3α and HLA-B*35:01. This accumulation of weaker distance-sensitive H-bond contacts is less tolerant of a P6-A substitution than the salt-bridge interaction of 3180, consequently the D1 TCR appears less responsive to NP1, 2 and 9-12 epitopes.

A recent study isolated 9 peptides presented by H-2L^{d} that were cross-recognized by the 43F3 TCR (*41*). Cross-recognition of 9 peptide variants of limited homology was achieved by re-arranging the CDR3β to engage with an "apical hot spot" situated in the peptides. In an *in vivo* context, HIV-1-infected individuals with cross-reactive TCRs (specific for the HLA-B*27:05-restricted KK10 epitope from HIV-1) able to recognize multiple HIV-1 variants can result in elite HIV-1 control (*42, 43*). Therefore, the cross-reactive TCRs analyzed in this study demonstrate a similar potential role for broad, CD8^{+} T cell-mediated protective immunity against diverse acute influenza viral infections.

Previous studies indicate that $NP_{418-426}$ conformation is heavily constrained, nevertheless we show that TCR recognition can be disrupted by establishing a combination of multiple but minor structural changes within the peptide epitope. The expansion of cross-reactive T cells capable of providing broad viral control will likely occur as populations undergo repeated infection by multiple related viruses. As each new viral strain infects an individual, it will trigger parallel expansion of naïve and memory T cell populations. As time progresses, this process could favor cross-reactive TCRs that preferentially target conserved positions upon the B*35:01/NP_{418} epitope. Here, we documented the clonotypic composition, cross-reactive potential and antigenic properties of TCRs that have the potential to provide universal protection against different influenza viruses. Research into the protective contribution and availability of equivalent TCRs at the population level are warranted.

Our conclusions are based on primary B35/NP_{418} T cell clones stimulated with peptide variants with the activation outcome measured by IFN-γ, TNF, CD107a and MIP-1β; primary T cell cultures for B35/NP_{418} viral variant cross-recognition with the use of NP_{418}-HLA-B*35:01 tetramers; and engineered Jurkat-TCR transfectants to define TCR recognition across several viral variants, using CD69 activation as a readout and NP_{418}-HLA-B*35:01 tetramer binding. While TCR transduction of human T cell lines is frequently used to provide key insights (e.g. (*32, 44, 45*), new immunological technologies have emerged, including CRISPR-Cas9-mediated orthotopic TCR-exchange in primary human T-cells (*46*) and these should be used in future studies.

MATERIALS AND METHODS

Study design. Our key question was to understand the mechanisms of cross-reactive TCR recognition towards a broad range of natural viral variants, specifically why some B35/NP_{418}-specific TCRs are more specific (or narrow) in recognition, while other TCRs display broader

recognition in the context of natural T cell variable antigens. We assessed the breadth of TCR recognition towards 12 natural influenza-derived NP_{418} viral variants and performed ternary structures of TCR-peptide-HLA-I complexes with naturally occurring viral variants (n=6 in our study) within one immunodominant viral epitope.

Human blood samples. Peripheral blood PBMCs from buffy packs (Melbourne Blood Bank, Australia) were isolated using Ficoll Paque (GE Healthcare, Sweden) density gradient and then cryopreserved. Healthy buffy pack donors (d1-d8) were aged between 30 to 66 years (average 44 years). Sex was collected for d3-d8 with 2 males and 4 females. Sex data was not collected for d1-d2 (table S8). HLA genotyping was performed by the Victorian Transplant and Immunogenetics Service (Melbourne, Australia). Human work was conducted according to the Declaration of Helsinki Principles and the Australian NHMRC Code of Practice. Signed informed consent was obtained from donors and the study was approved by the University of Melbourne Human Ethics Committee (ID1443389.3, ID1443540), and Australian Red Cross Blood Service (ARCBS) Ethics Committee (ID2015#8).

Expansion of peptide-specific $CD8^+$ T cells. PBMCs were incubated with specific peptides (Genscript, USA or Auspep, Australia) at 10μM in RPMI (Gibco, USA) as described (*17, 20, 21*). PBMC cultures were maintained for 11 days prior to the analysis of influenza-specific $CD8^+$ T cells. Primary $CD8^+$ T cell clones, generated previously by minimal dilution (*27*), were re-expanded by sorting live cells and stimulating for 48h with plate-bound anti-CD3 (UCHT1, 10 μg/ml), plate-bound anti-CD28 (CD28.2, 10 μg/ml, BD, USA), phytohemagglutinin (0.5 μg/ml; Sigma-Aldrich, USA), rhIL-2 (100 U/ml, PeproTech; USA), IL-7 (50 ng/ml, eBioscience, USA), IL-15 (50 ng/ml, PreproTech) followed by maintenance with IL-2, IL-7, IL-15 for 14–21 days.

HLA-B*35:01-NP_{418} tetramer staining. HLA-B*35:01-$NP_{418-426}$ and CD8-null biotinylated monomers were generated in the Rossjohn Laboratory at Monash University (Clayton, Australia) as per previous reports (*21, 47*). A gene encoding the extracellular domain of HLA-B*35:01 with the CD8 binding site mutations Q226K and D227A was designed and made synthetically with a Cterminal BirA tag (Genscript).

T cell lines were stained with HLA-B*35:01-$NP_{418-426}$ and/or HLA-B*35:01-NP_{418} CD8-null tetramers prepared by conjugation with streptavidin (SAv)-PE (BD) or SAv-BV-421 (Biolegend) at an 8:1 SAv to biotinylated monomer ratio. Cells were subsequently stained with Live/Dead-NIR (Life Technologies) followed by surface staining with the mAbs described

in table S9. Cells were analysed using a BD LSR Fortessa instrument or sorted using Aria III (Becton Dickinson, USA) or a MoFlo Astrios cell sorter (Beckman Coulter, USA).

Single-cell TCRαβ sequencing. Live $CD3^+$ $CD8^+$ T-cells were single-cell sorted and paired single-cell TCR αβ sequencing performed as described (*48, 49*). Briefly, cDNA was prepared using SuperScript VILO (Invitrogen, USA) and transcripts encoding Vα and Vβ genes were amplified by nested multiplex PCR. Sanger sequencing was performed by the Molecular Diagnostic Unit, University of Melbourne (Parkville, Australia). DNA chromatograms were analysed using FinchTV (Geospiza). TCR αβ genes and CDR3αβ regions were determined using the IMGT platform (*50*).

Generation of TCRαβ-expressing Jurkat76 (J76) cell lines and peptide stimulation. TCR constructs encoding full-length TCRα and TCRβ chains, separated by the cleavable 2A-linker, were synthesized (Geneart, Thermo, Germany) and inserted into the pMIGII plasmid. Cell lines expressing TCRαβ chains of interest were generated by retroviral transduction of TCRαβ-deficient J76 cells (Jurkat76 cell lines (human; T cell Leukaemia) lacking TCRαβ; a gift from Dr Zhenjun Chen, University of Melbourne, Australia) with TCR, 2A-cleavable CD3δεγζ and a CD8αβ constructs using HEK293T cells as virus packaging cells, as described (*51*). $2x10^5$ C1R-B*35:01$^+$ cells (kindly provided by Mandvi Bharadwaj, University of Melbourne, Australia) or negative control C1R-HLA-B*07:02 (kindly provided by Nicole Mifsud, Monash University, Australia) were incubated with the indicated amounts of peptide in RPMI for 1hr at 37°C and 5% CO_2. Peptide-treated cells were co-cultured overnight with $2x10^5$ TCR^+ J76 cells. Positive controls included J76 cells incubated with Phorbol myristate acetate (PMA; 10mg/mL) and Ionomycin (1μg/mL). Cells were then stained with Live/Dead-NIR followed by surface stained with mAbs listed.

Intracellular Cytokine Staining. Peptide-coated HLA-B*35:01$^+$ C1R targets were prepared as described (*20, 52*) and co-cultured with clonal $CD8^+$ T-cells at a 2:1 effector-to-target ratio using a minimum of $1x10^3$ effector cells, in the presence of Golgi Plug (1:1000, BD Biosciences) and anti-CD107a (eBioH4A3) for 4.5hrs. Cells were surfaced stained with mAbs listed in Table 2, followed by fixation and permeabilisation using the BD Cytofix/Cytoperm kit (BD, USA). Cells were intracellularly stained for cytokines with mAbs listed in Table 2.

Flow cytometry analyses. PBMC cultures and primary T cell clones were gated on single and live $CD3^+CD8^+$ T cells before gating on tetramer$^+$ cells, example shown in fig. S4A (bottom

left inset). Jurkat T cell clones were gated on CD8$\alpha\beta^+$ CD3^{high}GFP^{high} cells after doublet and dead cell exclusion and then analyzed for CD69 expression (Fig. 2A). Our tight gating strategy has been applied to analyse a homogenous population of CD3^{high}GFP^{high} CD8$\alpha\beta^+$ using the 293T TCR cell lines (human embryonic kidney cells; provided by McCluskey laboratory, University of Melbourne, Australia), as previously published by our laboratory and our collaborators (*53*). Using this approach, we can ensure that the expression levels of CD8 and TCR (GFP/CD3) for each sample stained with distinct tetramers are matched, thereby removing these factors as confounding variables in the analysis of tetramer staining intensity. Primary T cell clones were gated on CD3$^+$CD8$^+$ T cells after doublet and dead cell exclusion for the ICS as shown in fig. S7. All data were processed using FlowJo software (Treestar).

Transient surface molecule expression. 293T cells were seeded in 6-well plates and incubated overnight at 37 °C and 5% CO_2. Cells were transfected with TCR$\alpha\beta$, 2A-cleavable CD3εδγζ and a CD8αβ constructs using FuGene (Promega, USA) according to the manufacturer's instructions. Transfected cells were stained with HLA-B*35:01/NP_{418}-specific tetramers and antibodies listed in table S9.

Generation of soluble TCRs and HLA-B*35:01. The D1 and 3180 TCRs were expressed in *E. coli* as inclusion bodies, before being refolded using an engineered disulphide linkage in the constant domains between the TRAC and TRBC, as previously described (*54*). The TCRs were then purified in 10 mM Tris-HCl pH 8, 150 mM NaCl, and proper folding was assessed using conformational antibodies (*55*). Soluble HLA-B:35*01 heterodimers containing the NP_{418} peptides variants were prepared as described (*20*).

Crystallization, structure determination and refinement

Crystals of the HLA-B*35:01-NP_{418} complexes and TCR-pHLA were obtained as described (*20*). Data were collected on the MX1 and MX2 beamlines at the Australian Synchrotron (*56*) using the ADSC-Quantum 210, 315r CCD or Eiger 6M detectors (at 100K). Data were processed using XDS (*57*) and scaled using Aimless from the CCP4 suite (*58*). The structures were determined by molecular replacement using the PHASER program (*59*) with the LC13 TCR as the search model for the TCR (PDB: 3KPS (*60*) and the LPFEKSTVM/HLA-B:35*01 for the HLA model without the peptide (Protein Data Bank accession number, 3LKS (*20*). Manual model building was conducted using Coot (*61*)) followed by maximum-likelihood refinement with the Buster program (*62*). The TCRs were numbered according to the IMGT unique numbering system (*63*). The final model has been validated using the Protein Data

Base validation web site and the final refinement statistics are summarized in tables S3-S4. Coordinates were submitted to PDB database with the accession codes: 8EMK for HLA-B*3501-NP3; 8EMF for HLA-B*3501-NP6; 8EMG for HLA-B*3501-NP7; 8EMI for HLA-B*3501-NP8; 8EMJ for HLA-B*3501-NP9; 8EN8 for 3180-HLA-B*3501-NP4; 8ENH for 3180-HLA-B*3501-NP7; 8EO8 for 3180-HLA-B*3501-NP8; 8V50 for D1-HLA-B*3501-NP6; 8V4Z for D1-HLA-B*3501-NP7; 8V51 for D1-HLA-B*3501-NP10.

Surface Plasmon Resonance.

Surface plasmon resonance experiments were conducted at 25 °C on the BIAcore 3000 instrument (GE Healthcare, Buckinghamshire, UK) with 0.1 M Tris-HCl pH8, 0.15 M NaCl buffer supplemented with 0.5% bovine serum albumin to prevent non-specific binding as previously described (*64*). Briefly, the TCRs D1 and 3180 were coupled to the sensor chip via the monoclonal antibody 12H8[32] and HLA-B*35:01 presenting the different NP_{418} variants were injected over the surface with a maximum concentration of 200 µM. BIAevaluation Version 3.1 was used for data analysis with the 1:1 Langmuir binding model, and the results are summarised in table S1.

Statistical analysis

One-way ANOVA followed by Tukey post-test was performed for comparisons between responses towards different NP_{418} variants.

SUPPLEMENTARY MATERIALS

Figure S1. LILRB1-expressing Ba/F3 cells stained with B*35:01-NP_{418}-PE or B*35:01-NP_{418}-BV421.

Figure S2. Flow cytometry profiles of distinct dual B*35:01/NP_{418}-PE and B*35:01-NP_{418}-BV421 tetramer staining for a representative d1 donor.

Figure S3. Validation of B*35:01/NP_{418}-tetramer and confirmation of TCR reactivity.

Figure S4. Flow cytometry profiles of dual B*35:01/NP_{418}-PE and B*35:01-NP_{418}-BV421 tetramer staining using WT and NULL tetramers.

Figure S5. HLA-B*35:01-NP_{418} variant structures.

Figure S6. 3180 and D1 TCR-pHLA ternary structures.

Figure S7. Gating strategy for primary T cell clones.

Table S1. Surface Plasmon Resonance: affinity measurements of D1 and 3180 TCRs.

Table S2. HLA-B*35:01-NP_{418} CD8-null tetramers generated for the assessment of cross-reactive responses independent of CD8β co-receptor binding.

Table S3. Data collection and refinement statistics for the peptide-HLA structures.

Table S4. Data collection and refinement statistics for the TCR-pHLA complex structures.

Table S5. Contribution to buried surface area of TCR: peptide-HLA complexes (*65*).

Table S6. D1 TCR contacts with HLA-B*35:01 presenting variants NP6, NP7 and NP10.

Table S7. 3180 TCR contacts with HLA-B*35:01 presenting variants NP4, NP7 and NP8.

Table S8. Healthy buffy pack donor age, sex and HLA typing.

Table S9. Anti-human monoclonal antibodies used for flow cytometry.

Data File s1. Raw data

REFERENCES:

1. A. J. McMichael, F. M. Gotch, G. R. Noble, P. A. Beare, Cytotoxic T-cell immunity to influenza. . *New Eng J Med* **309**, 13-17 (1983).
2. S. Sridhar, S. Begom, A. Bermingham, K. Hoschler, W. Adamson, W. Carman, T. Bean, W. Barclay, J. J. Deeks, A. Lalvani, Cellular immune correlates of protection against symptomatic pandemic influenza. *Nat Med* **19** 1305-1312 (2013).
3. A. C. Hayward, L. Wang, N. Goonetilleke, E. B. Fragaszy, A. Bermingham, A. Copas, O. Dukes, E. R. Millett, I. Nazareth, J. S. Nguyen-Van-Tam, J. M. Watson, M. Zambon, A. M. Johnson, A. J. McMichael, G. Flu Watch, Natural T Cell-mediated Protection against Seasonal and Pandemic Influenza. Results of the Flu Watch Cohort Study. *American journal of respiratory and critical care medicine* **191**, 1422-1431 (2015).
4. Z. Wang, Y. Wan, C. Qiu, Z. Zhu, S. Quinones-Parra, L. Loh, D. Tian, Y. Ren, Y. Hu, X. Zhang, P. G. Thomas, M. Inouye, P. C. Doherty, K. Kedzierska, J. Xu, Recovery from severe H7N9 disease is associated with diverse response mechanisms driven by CD8+ T cells. *Nat Commun* **6:6833. doi: 10.1038/ncomms7833**, (2015).
5. A. Jozwik, M. S. Habibi, A. Paras, J. Zhu, A. Guvenel, J. Dhariwal, M. Almond, E. H. C. Wong, A. Sykes, M. Maybeno, J. Del Rosario, M. B. Trujillo-Torralbo, P. Mallia, J. Sidney, B. Peters, O. M. Kon, A. Sette, S. L. Johnston, P. J. Openshaw, C. Chiu, RSV-specific airway resident memory CD8+ T cells and differential disease severity after experimental human infection. *Nat Commun* **6**, 10224 (2015).
6. Y. Peng, S. L. Felce, D. Dong, F. Penkava, A. J. Mentzer, X. Yao, G. Liu, Z. Yin, J. L. Chen, Y. Lu, D. Wellington, P. A. C. Wing, D. C. C. Dominey-Foy, C. Jin, W. Wang, M. A. Hamid, R. A. Fernandes, B. Wang, A. Fries, X. Zhuang, N. Ashley, T. Rostron, C. Waugh, P. Sopp, P. Hublitz, R. Beveridge, T. K. Tan, C. Dold, A. J. Kwok, C. Rich-Griffin, W. Dejnirattisa, C. Liu, P. Kurupati, I. Nassiri, R. A. Watson, O. Tong, C. A. Taylor, P. Kumar Sharma, B. Sun, F. Curion, S. Revale, L. C. Garner, K. Jansen, R. C. Ferreira, M. Attar, J. W. Fry, R. A. Russell, C. Consortium, H. J. Stauss, W. James, A. Townsend, L. P. Ho, P. Klenerman, J. Mongkolsapaya, G. R. Screaton, C. Dendrou, S. N. Sansom, R. Bashford-Rogers, B. Chain, G. L. Smith, J. A. McKeating, B. P. Fairfax, P. Bowness, A. J. McMichael, G. Ogg, J. C. Knight, T. Dong, An immunodominant NP105-113-B*07:02 cytotoxic T cell response controls viral replication and is associated with less severe COVID-19 disease. *Nat Immunol*, (2021).
7. D. G. Augusto, L. D. Murdolo, D. S. M. Chatzileontiadou, J. J. Sabatino, Jr., T. Yusufali, N. D. Peyser, X. Butcher, K. Kizer, K. Guthrie, V. W. Murray, V. Pae, S. Sarvadhavabhatla, F. Beltran, G. S. Gill, K. L. Lynch, C. Yun, C. T. Maguire, M. J. Peluso, R. Hoh, T. J. Henrich, S. G. Deeks, M. Davidson, S. Lu, S. A. Goldberg, J. D. Kelly, J. N. Martin, C. A. Vierra-Green, S. R. Spellman, D. J. Langton, M. J. Dewar-

Oldis, C. Smith, P. J. Barnard, S. Lee, G. M. Marcus, J. E. Olgin, M. J. Pletcher, M. Maiers, S. Gras, J. A. Hollenbach, A common allele of HLA is associated with asymptomatic SARS-CoV-2 infection. *Nature* **620**, 128-136 (2023).
8. R. C. Mettelman, A. Souquette, L. A. Van de Velde, K. Vegesana, E. K. Allen, C. M. Kackos, S. Trifkovic, J. DeBeauchamp, T. L. Wilson, D. G. St James, S. S. Menon, T. Wood, L. Jelley, R. J. Webby, Q. S. Huang, P. G. Thomas, S.-I. I. Team, Baseline innate and T cell populations are correlates of protection against symptomatic influenza virus infection independent of serology. *Nat Immunol* **24**, 1511-1526 (2023).
9. M. Z. M. Zheng, T. K. Tan, F. Villalon-Letelier, H. Lau, Y. M. Deng, S. Fritzlar, S. A. Valkenburg, H. Gu, L. L. M. Poon, P. C. Reading, A. R. Townsend, L. M. Wakim, Single-cycle influenza virus vaccine generates lung CD8(+) Trm that cross-react against viral variants and subvert virus escape mutants. *Sci Adv* **9**, eadg3469 (2023).
10. I. Uddback, S. E. Michalets, A. Saha, C. Mattingly, K. N. Kost, M. E. Williams, L. A. Lawrence, S. L. Hicks, A. C. Lowen, H. Ahmed, A. R. Thomsen, C. J. Russell, C. D. Scharer, J. M. Boss, K. Koelle, R. Antia, J. P. Christensen, J. E. Kohlmeier, Prevention of respiratory virus transmission by resident memory CD8(+) T cells. *Nature* **626**, 392-400 (2024).
11. K. McMahan, J. Yu, N. B. Mercado, C. Loos, L. H. Tostanoski, A. Chandrashekar, J. Liu, L. Peter, C. Atyeo, A. Zhu, E. A. Bondzie, G. Dagotto, M. S. Gebre, C. Jacob-Dolan, Z. Li, F. Nampanya, S. Patel, L. Pessaint, A. Van Ry, K. Blade, J. Yalley-Ogunro, M. Cabus, R. Brown, A. Cook, E. Teow, H. Andersen, M. G. Lewis, D. A. Lauffenburger, G. Alter, D. H. Barouch, Correlates of protection against SARS-CoV-2 in rhesus macaques. *Nature* **590**, 630-634 (2021).
12. E. M. Bange, N. A. Han, P. Wileyto, J. Y. Kim, S. Gouma, J. Robinson, A. R. Greenplate, M. A. Hwee, F. Porterfield, O. Owoyemi, K. Naik, C. Zheng, M. Galantino, A. R. Weisman, C. A. G. Ittner, E. M. Kugler, A. E. Baxter, O. Oniyide, R. S. Agyekum, T. G. Dunn, T. K. Jones, H. M. Giannini, M. E. Weirick, C. M. McAllister, N. E. Babady, A. Kumar, A. J. Widman, S. DeWolf, S. R. Boutemine, C. Roberts, K. R. Budzik, S. Tollett, C. Wright, T. Perloff, L. Sun, D. Mathew, J. R. Giles, D. A. Oldridge, J. E. Wu, C. Alanio, S. Adamski, A. L. Garfall, L. A. Vella, S. J. Kerr, J. V. Cohen, R. A. Oyer, R. Massa, I. P. Maillard, K. N. Maxwell, J. P. Reilly, P. G. Maslak, R. H. Vonderheide, J. D. Wolchok, S. E. Hensley, E. J. Wherry, N. J. Meyer, A. M. DeMichele, S. A. Vardhana, R. Mamtani, A. C. Huang, CD8(+) T cells contribute to survival in patients with COVID-19 and hematologic cancer. *Nat Med* **27**, 1280-1289 (2021).
13. S. M. Quinones-Parra, E. B. Clemens, Z. Wang, H. A. Croom, L. Kedzierski, J. McVernon, D. Vijaykrishna, K. Kedzierska, A Role of Influenza Virus Exposure History in Determining Pandemic Susceptibility and CD8+ T Cell Responses. *J Virol* **90**, 6936-6947 (2016).
14. M. Z. M. Zheng, L. M. Wakim, Tissue resident memory T cells in the respiratory tract. *Mucosal Immunol* **15**, 379-388 (2022).
15. K. Kedzierska, P. G. Thomas, Count on us: T cells in SARS-CoV-2 infection and vaccination. *Cell Rep Med* **3**, 100562 (2022).
16. L. C. Rowntree, T. H. O. Nguyen, L. Kedzierski, M. R. Neeland, J. Petersen, J. C. Crawford, L. F. Allen, E. B. Clemens, B. Chua, H. A. McQuilten, A. A. Minervina, M. V. Pogorelyy, P. Chaurasia, H. X. Tan, A. K. Wheatley, X. Jia, F. Amanat, F. Krammer, E. K. Allen, S. Sonda, K. L. Flanagan, J. Jumarang, P. S. Pannaraj, P. V. Licciardi, S. J. Kent, K. A. Bond, D. A. Williamson, J. Rossjohn, P. G. Thomas, S. Tosif, N. W. Crawford, C. E. van de Sandt, K. Kedzierska, SARS-CoV-2-specific T cell memory with common TCRalphabeta motifs is established in unvaccinated children who seroconvert after infection. *Immunity* **55**, 1299-1315 e1294 (2022).
17. S. Quinones-Parra, E. Grant, L. Loh, T. H. Nguyen, K. A. Campbell, S. Y. Tong, A. Miller, P. C. Doherty, D. Vijaykrishna, J. Rossjohn, S. Gras, K. Kedzierska, Preexisting

CD8+ T-cell immunity to the H7N9 influenza A virus varies across ethnicities. *Proc Natl Acad Sci U S A* **111**, 1049-1054 (2014).
18. M. Koutsakos, P. Illing, T. Nguyen, N. Mifsud, J. Crawford, S. Rizzetto, A. Eltahla, E. B. Clemens, S. Sant, B. Chua, C. Wong, E. Allen, D. Teng, P. Dash, D. Boyd, L. Grzelak, W. Zeng, A. Hurt, I. Barr, S. Rockman, D. Jackson, T. Kotsimbos, A. Cheng, M. Richards, G. Westall, T. Loudovaris, S. Mannering, M. Elliot, S. Tangye, L. Wakim, J. Rossjohn, D. Vijaykrishna, F. Luciani, P. Thomas, S. Gras, A. Purcell, K. Kedzierska, Human CD8+ T cell cross-reactivity across influenza A, B and C viruses *Nature Immunology* **20**, 613-625 (2019).
19. L. Hensen, P. T. Illing, E. Bridie Clemens, T. H. O. Nguyen, M. Koutsakos, C. E. van de Sandt, N. A. Mifsud, A. T. Nguyen, C. Szeto, B. Y. Chua, H. Halim, S. Rizzetto, F. Luciani, L. Loh, E. J. Grant, P. M. Saunders, A. G. Brooks, S. Rockman, T. C. Kotsimbos, A. C. Cheng, M. Richards, G. P. Westall, L. M. Wakim, T. Loudovaris, S. I. Mannering, M. Elliott, S. G. Tangye, D. C. Jackson, K. L. Flanagan, J. Rossjohn, S. Gras, J. Davies, A. Miller, S. Y. C. Tong, A. W. Purcell, K. Kedzierska, CD8(+) T cell landscape in Indigenous and non-Indigenous people restricted by influenza mortality-associated HLA-A*24:02 allomorph. *Nat Commun* **12**, 2931 (2021).
20. S. Gras, L. Kedzierski, S. A. Valkenburg, K. Laurie, Y. C. Liu, J. T. Denholm, M. J. Richards, G. F. Rimmelzwaan, A. Kelso, P. C. Doherty, S. J. Turner, J. Rossjohn, K. Kedzierska, Cross-reactive CD8+ T-cell immunity between the pandemic H1N1-2009 and H1N1-1918 influenza A viruses. *Proc Natl Acad Sci U S A* **107**, 12599-12604 (2010).
21. S. A. Valkenburg, T. M. Josephs, E. B. Clemens, E. J. Grant, T. H. Nguyen, G. C. Wang, D. A. Price, A. Miller, S. Y. Tong, P. G. Thomas, P. C. Doherty, J. Rossjohn, S. Gras, K. Kedzierska, Molecular basis for universal HLA-A*0201-restricted CD8+ T-cell immunity against influenza viruses. *Proc Natl Acad Sci U S A* **113**, 4440-4445 (2016).
22. D. K. Cole, A. M. Bulek, G. Dolton, A. J. Schauenberg, B. Szomolay, W. Rittase, A. Trimby, P. Jothikumar, A. Fuller, A. Skowera, J. Rossjohn, C. Zhu, J. J. Miles, M. Peakman, L. Wooldridge, P. J. Rizkallah, A. K. Sewell, Hotspot autoimmune T cell receptor binding underlies pathogen and insulin peptide cross-reactivity. *J Clin Invest* **126**, 2191-2204 (2016).
23. X. Yang, L. I. Garner, I. V. Zvyagin, M. A. Paley, E. A. Komech, K. M. Jude, X. Zhao, R. A. Fernandes, L. M. Hassman, G. L. Paley, C. S. Savvides, S. Brackenridge, M. N. Quastel, D. M. Chudakov, P. Bowness, W. M. Yokoyama, A. J. McMichael, G. M. Gillespie, K. C. Garcia, Autoimmunity-associated T cell receptors recognize HLA-B*27-bound peptides. *Nature* **612**, 771-777 (2022).
24. G. Dolton, C. Rius, A. Wall, B. Szomolay, V. Bianchi, S. A. E. Galloway, M. S. Hasan, T. Morin, M. E. Caillaud, H. L. Thomas, S. Theaker, L. R. Tan, A. Fuller, K. Topley, M. Legut, M. Attaf, J. R. Hopkins, E. Behiry, J. Zabkiewicz, C. Alvares, A. Lloyd, A. Rogers, P. Henley, C. Fegan, O. Ottmann, S. Man, M. D. Crowther, M. Donia, I. M. Svane, D. K. Cole, P. E. Brown, P. Rizkallah, A. K. Sewell, Targeting of multiple tumor-associated antigens by individual T cell receptors during successful cancer immunotherapy. *Cell* **186**, 3333-3349 e3327 (2023).
25. D. K. Cole, H. A. van den Berg, A. Lloyd, M. D. Crowther, K. Beck, J. Ekeruche-Makinde, J. J. Miles, A. M. Bulek, G. Dolton, A. J. Schauenburg, A. Wall, A. Fuller, M. Clement, B. Laugel, P. J. Rizkallah, L. Wooldridge, A. K. Sewell, Structural Mechanism Underpinning Cross-reactivity of a CD8+ T-cell Clone That Recognizes a Peptide Derived from Human Telomerase Reverse Transcriptase. *J Biol Chem* **292**, 802-813 (2017).
26. A. C. Boon, G. de Mutsert, Y. M. Graus, R. A. Fouchier, K. Sintnicolaas, A. D. Osterhaus, G. F. Rimmelzwaan, Sequence variation in a newly identified HLA-B35-

restricted epitope in the influenza A virus nucleoprotein associated with escape from cytotoxic T lymphocytes. *J Virol* **76**, 2567-2572 (2002).
27. A. C. Boon, G. de Mutsert, D. van Baarle, D. J. Smith, A. S. Lapedes, R. A. Fouchier, K. Sintnicolaas, A. D. Osterhaus, G. F. Rimmelzwaan, Recognition of homo- and heterosubtypic variants of influenza A viruses by human CD8+ T lymphocytes. *J Immunol* **172**, 2453-2460 (2004).
28. A. C. Boon, E. Fringuelli, Y. M. Graus, R. A. Fouchier, K. Sintnicolaas, A. M. Iorio, G. F. Rimmelzwaan, A. D. Osterhaus, Influenza A virus specific T cell immunity in humans during aging. *Virology* **299**, 100-108 (2002).
29. D. Middleton, L. Menchaca, H. Rood, R. Komerofsky, New Allele Frequency Database: http://www.allelefrequencies.net. *Tissue Antigens* **61**, 403-407 (2003).
30. A. Wahl, F. Schafer, W. Bardet, R. Buchli, G. M. Air, W. H. Hildebrand, HLA class I molecules consistently present internal influenza epitopes. *Proc Natl Acad Sci U S A* **106**, 540-545 (2009).
31. E. B. Clemens, E. J. Grant, Z. Wang, S. Gras, P. Tipping, J. Rossjohn, A. Miller, S. Y. Tong, K. Kedzierska, Towards identification of immune and genetic correlates of severe influenza disease in Indigenous Australians. *Immunol Cell Biol* **94**, 367-377 (2016).
32. C. E. van de Sandt, T. H. O. Nguyen, N. A. Gherardin, J. C. Crawford, J. Samir, A. A. Minervina, M. V. Pogorelyy, S. Rizzetto, C. Szeto, J. Kaur, N. Ranson, S. Sonda, A. Harper, S. J. Redmond, H. A. McQuilten, T. Menon, S. Sant, X. Jia, K. Pedrina, T. Karapanagiotidis, N. Cain, S. Nicholson, Z. Chen, R. Lim, E. B. Clemens, A. Eltahla, N. L. La Gruta, J. Crowe, M. Lappas, J. Rossjohn, D. I. Godfrey, P. G. Thomas, S. Gras, K. L. Flanagan, F. Luciani, K. Kedzierska, Newborn and child-like molecular signatures in older adults stem from TCR shifts across human lifespan. *Nat Immunol* **24**, 1890-1907 (2023).
33. N. L. La Gruta, P. C. Doherty, S. J. Turner, A correlation between function and selected measures of T cell avidity in influenza virus-specific CD8+ T cell responses. *Eur J Immunol* **36**, 2951-2959 (2006).
34. E. J. Grant, T. M. Josephs, S. A. Valkenburg, L. Wooldridge, M. Hellard, J. Rossjohn, M. Bharadwaj, K. Kedzierska, S. Gras, Lack of Heterologous Cross-reactivity toward HLA-A*02:01 Restricted Viral Epitopes Is Underpinned by Distinct alphabetaT Cell Receptor Signatures. *J Biol Chem* **291**, 24335-24351 (2016).
35. Z. Wang, Y. Wan, C. Qiu, S. Quinones-Parra, Z. Zhu, L. Loh, D. Tian, Y. Ren, Y. Hu, X. Zhang, P. G. Thomas, M. Inouye, P. C. Doherty, K. Kedzierska, J. Xu, Recovery from severe H7N9 disease is associated with diverse response mechanisms dominated by CD8(+) T cells. *Nat Commun* **6**, 6833 (2015).
36. Z. Wang, L. Zhu, T. H. O. Nguyen, Y. Wan, S. Sant, S. M. Quinones-Parra, J. C. Crawford, A. A. Eltahla, S. Rizzetto, R. A. Bull, C. Qiu, M. Koutsakos, E. B. Clemens, L. Loh, T. Chen, L. Liu, P. Cao, Y. Ren, L. Kedzierski, T. Kotsimbos, J. M. McCaw, N. L. La Gruta, S. J. Turner, A. C. Cheng, F. Luciani, X. Zhang, P. C. Doherty, P. G. Thomas, J. Xu, K. Kedzierska, Clonally diverse CD38(+)HLA-DR(+)CD8(+) T cells persist during fatal H7N9 disease. *Nat Commun* **9**, 824 (2018).
37. X. Jia, B. Y. Chua, L. Loh, M. Koutsakos, L. Kedzierski, M. Olshansky, W. R. Heath, S. Y. Chang, J. Xu, Z. Wang, K. Kedzierska, High expression of CD38 and MHC class II on CD8(+) T cells during severe influenza disease reflects bystander activation and trogocytosis. *Clin Transl Immunology* **10**, e1336 (2021).
38. R. C. Mettelman, E. K. Allen, P. G. Thomas, Mucosal immune responses to infection and vaccination in the respiratory tract. *Immunity* **55**, 749-780 (2022).
39. A. Wahl, W. McCoy, F. Schafer, W. Bardet, R. Buchli, D. H. Fremont, W. H. Hildebrand, T-cell tolerance for variability in an HLA class I-presented influenza A virus epitope. *J Virol* **83**, 9206-9214 (2009).

40. J. Sidney, B. Peters, N. Frahm, C. Brander, A. Sette, HLA class I supertypes: a revised and updated classification. *BMC Immunol* **9**, 1 (2008).
41. J. J. Adams, S. Narayanan, M. E. Birnbaum, S. S. Sidhu, S. J. Blevins, M. H. Gee, L. V. Sibener, B. M. Baker, D. M. Kranz, K. C. Garcia, Structural interplay between germline interactions and adaptive recognition determines the bandwidth of TCR-peptide-MHC cross-reactivity. *Nat Immunol* **17**, 87-94 (2016).
42. K. Ladell, M. Hashimoto, M. C. Iglesias, P. G. Wilmann, J. E. McLaren, S. Gras, T. Chikata, N. Kuse, S. Fastenackels, E. Gostick, J. S. Bridgeman, V. Venturi, Z. A. Arkoub, H. Agut, D. J. van Bockel, J. R. Almeida, D. C. Douek, L. Meyer, A. Venet, M. Takiguchi, J. Rossjohn, D. A. Price, V. Appay, A molecular basis for the control of preimmune escape variants by HIV-specific CD8+ T cells. *Immunity* **38**, 425-436 (2013).
43. H. Chen, Z. M. Ndhlovu, D. Liu, L. C. Porter, J. W. Fang, S. Darko, M. A. Brockman, T. Miura, Z. L. Brumme, A. Schneidewind, A. Piechocka-Trocha, K. T. Cesa, J. Sela, T. D. Cung, I. Toth, F. Pereyra, X. G. Yu, D. C. Douek, D. E. Kaufmann, T. M. Allen, B. D. Walker, TCR clonotypes modulate the protective effect of HLA class I molecules in HIV-1 infection. *Nature immunology* **13**, 691-700 (2012).
44. W. Awad, G. J. M. Ler, W. Xu, A. N. Keller, J. Y. W. Mak, X. Y. Lim, L. Liu, S. B. G. Eckle, J. Le Nours, J. McCluskey, A. J. Corbett, D. P. Fairlie, J. Rossjohn, The molecular basis underpinning the potency and specificity of MAIT cell antigens. *Nat Immunol* **21**, 400-411 (2020).
45. J. J. Lim, C. M. Jones, T. J. Loh, Y. T. Ting, P. Zareie, K. L. Loh, N. J. Felix, A. Suri, M. McKinnon, F. Stevenaert, R. K. Sharma, L. Klareskog, V. Malmstrom, D. G. Baker, A. W. Purcell, H. H. Reid, N. L. La Gruta, J. Rossjohn, The shared susceptibility epitope of HLA-DR4 binds citrullinated self-antigens and the TCR. *Sci Immunol* **6**, (2021).
46. S. A. Oh, K. Senger, S. Madireddi, I. Akhmetzyanova, I. E. Ishizuka, S. Tarighat, J. H. Lo, D. Shaw, B. Haley, S. Rutz, High-efficiency nonviral CRISPR/Cas9-mediated gene editing of human T cells using plasmid donor DNA. *J Exp Med* **219**, (2022).
47. T. H. O. Nguyen, M. Koutsakos, C. E. van de Sandt, J. C. Crawford, L. Loh, S. Sant, L. Grzelak, E. K. Allen, T. Brahm, E. B. Clemens, M. Auladell, L. Hensen, Z. Wang, S. Nussing, X. Jia, P. Gunther, A. K. Wheatley, S. J. Kent, M. Aban, Y. M. Deng, K. L. Laurie, A. C. Hurt, S. Gras, J. Rossjohn, J. Crowe, J. Xu, D. Jackson, L. E. Brown, N. La Gruta, W. Chen, P. C. Doherty, S. J. Turner, T. C. Kotsimbos, P. G. Thomas, A. C. Cheng, K. Kedzierska, Immune cellular networks underlying recovery from influenza virus infection in acute hospitalized patients. *Nat Commun* **12**, 2691 (2021).
48. Y. Zhao, Y. H. Zhang, L. Denney, D. Young, T. J. Powell, Y. C. Peng, N. Li, H. P. Yan, D. Y. Wang, Y. L. Shu, Y. Kendrick, A. J. McMichael, L. P. Ho, T. Dong, High levels of virus-specific CD4+ T cells predict severe pandemic influenza A virus infection. *American journal of respiratory and critical care medicine* **186**, 1292-1297 (2012).
49. T. H. Nguyen, A. C. Tan, S. D. Xiang, A. Goubier, K. L. Harland, E. B. Clemens, M. Plebanski, K. Kedzierska, Understanding CD8(+) T-cell responses toward the native and alternate HLA-A*02:01-restricted WT1 epitope. *Clin Transl Immunology* **6**, e134 (2017).
50. A. L. Marzo, K. D. Klonowski, A. Le Bon, P. Borrow, D. F. Tough, L. Lefrancois, Initial T cell frequency dictates memory CD8+ T cell lineage commitment. *Nat Immunol* **6**, 793-799 (2005).
51. J. Holst, K. M. Vignali, A. R. Burton, D. A. Vignali, Rapid analysis of T-cell selection in vivo using T cell-receptor retrogenic mice. *Nat Methods* **3**, 191-197 (2006).
52. E. B. Clemens, E. J. Grant, Z. Wang, S. Gras, P. Tipping, J. Rossjohn, A. Miller, S. Y. C. Tong, K. Kedzierska, Towards identification of immune and genetic correlates of severe influenza disease in Indigenous Australians. *Immunol Cell Biol* **95**, 648 (2017).

53. N. A. Gherardin, S. J. Redmond, H. E. G. McWilliam, C. F. Almeida, K. H. A. Gourley, R. Seneviratna, S. Li, R. De Rose, F. J. Ross, C. V. Nguyen-Robertson, S. Su, M. E. Ritchie, J. A. Villadangos, D. B. Moody, D. G. Pellicci, A. P. Uldrich, D. I. Godfrey, CD36 family members are TCR-independent ligands for CD1 antigen-presenting molecules. *Sci Immunol* **6**, (2021).
54. C. S. Clements, L. Kjer-Nielsen, W. A. MacDonald, A. G. Brooks, A. W. Purcell, J. McCluskey, J. Rossjohn, The production, purification and crystallization of a soluble heterodimeric form of a highly selected T-cell receptor in its unliganded and liganded state. *Acta Crystallogr D Biol Crystallogr* **58**, 2131-2134 (2002).
55. N. A. Borg, L. K. Ely, T. Beddoe, W. A. Macdonald, H. H. Reid, C. S. Clements, A. W. Purcell, L. Kjer-Nielsen, J. J. Miles, S. R. Burrows, J. McCluskey, J. Rossjohn, The CDR3 regions of an immunodominant T cell receptor dictate the 'energetic landscape' of peptide-MHC recognition. *Nat Immunol* **6**, 171-180 (2005).
56. D. Aragao, J. Aishima, H. Cherukuvada, R. Clarken, M. Clift, N. P. Cowieson, D. J. Ericsson, C. L. Gee, S. Macedo, N. Mudie, S. Panjikar, J. R. Price, A. Riboldi-Tunnicliffe, R. Rostan, R. Williamson, T. T. Caradoc-Davies, MX2: a high-flux undulator microfocus beamline serving both the chemical and macromolecular crystallography communities at the Australian Synchrotron. *J Synchrotron Radiat* **25**, 885-891 (2018).
57. W. Kabsch, Integration, scaling, space-group assignment and post-refinement. *Acta Crystallogr D Biol Crystallogr* **66**, 133-144 (2010).
58. The CCP4 suite: programs for protein crystallography. *Acta Crystallogr D Biol Crystallogr* **50**, 760-763 (1994).
59. R. J. Read, Pushing the boundaries of molecular replacement with maximum likelihood. *Acta Crystallogr D Biol Crystallogr* **57**, 1373-1382 (2001).
60. W. A. Macdonald, A. W. Purcell, N. A. Mifsud, L. K. Ely, D. S. Williams, L. Chang, J. J. Gorman, C. S. Clements, L. Kjer-Nielsen, D. M. Koelle, S. R. Burrows, B. D. Tait, R. Holdsworth, A. G. Brooks, G. O. Lovrecz, L. Lu, J. Rossjohn, J. McCluskey, A naturally selected dimorphism within the HLA-B44 supertype alters class I structure, peptide repertoire, and T cell recognition. *J Exp Med* **198**, 679-691 (2003).
61. P. Emsley, K. Cowtan, Coot: model-building tools for molecular graphics. *Acta Crystallogr D Biol Crystallogr* **60**, 2126-2132 (2004).
62. O. S. Smart, T. O. Womack, C. Flensburg, P. Keller, W. Paciorek, A. Sharff, C. Vonrhein, G. Bricogne, Exploiting structure similarity in refinement: automated NCS and target-structure restraints in BUSTER. *Acta Crystallogr D Biol Crystallogr* **68**, 368-380 (2012).
63. M. P. Lefranc, C. Pommie, Q. Kaas, E. Duprat, N. Bosc, D. Guiraudou, C. Jean, M. Ruiz, I. Da Piedade, M. Rouard, E. Foulquier, V. Thouvenin, G. Lefranc, IMGT unique numbering for immunoglobulin and T cell receptor constant domains and Ig superfamily C-like domains. *Dev Comp Immunol* **29**, 185-203 (2005).
64. S. Gras, S. R. Burrows, L. Kjer-Nielsen, C. S. Clements, Y. C. Liu, L. C. Sullivan, M. J. Bell, A. G. Brooks, A. W. Purcell, J. McCluskey, J. Rossjohn, The shaping of T cell receptor recognition by self-tolerance. *Immunity* **30**, 193-203 (2009).
65. J. Rossjohn, S. Gras, J. J. Miles, S. J. Turner, D. I. Godfrey, J. McCluskey, T cell antigen receptor recognition of antigen-presenting molecules. *Annu Rev Immunol* **33**, 169-200 (2015).

Acknowledgments:

We thank Dr Dale Godfrey for stimulating discussions.

Funding: This work was supported by NHMRC: L1 to K.K. (#1173871), EL1 to T.H.O.N. (#1194036), EL1 to L.C.R (#2026357), SRFA to S.G. (#1159272). J.R. is supported by an NHMRC Investigator Award. S.M.Q.-P. was a recipient of the University of Melbourne International Research Scholarship and a Consejo Nacional de Ciencia y Tecnología Scholar. S.S. was supported by the Victoria-India Doctoral Scholarship (VIDS) and the Melbourne International Fee Remission Scholarship (MIFRS). This work was supported by Research Grants Council of the Hong Kong Special Administrative Region, China (#T11-712/19-N) to K.K. This research was undertaken in part using the MX2 beamline at the Australian Synchrotron, part of ANSTO, and made use of the Australian Cancer Research Foundation (ACRF) detector.

Author Contributions: K.K. and J.R. supervised the study. S.M.Q.-P., S.G., J.R. and K.K. designed the experiments. S.M.Q.-P., S.G., C.F., C.S., T.H.O.N., S.S., D.J., L.C.R., P.C., J.P. and D.R.L. performed and analysed experiments. A.C.M.B. and G.R. provided crucial reagents. P.C.D., and A.P.U. provided intellectual input. S.M.Q.-P., S.G., T.H.O.N., J.R. and K.K. wrote the manuscript. All authors reviewed and approved the manuscript.

Competing interests: The authors declare that they have no competing interests.

Data and materials availability: The data for this study have been deposited in the PDB database with the accession codes: 8EMK for HLA-B*3501-NP3; 8EMF for HLA-B*3501-NP6; 8EMG for HLA-B*3501-NP7; 8EMI for HLA-B*3501-NP8; 8EMJ for HLA-B*3501-NP9; 8EN8 for 3180-HLA-B*3501-NP4; 8ENH for 3180-HLA-B*3501-NP7; 8EO8 for 3180-HLA-B*3501-NP8; 8V50 for D1-HLA-B*3501-NP6; 8V4Z for D1-HLA-B*3501-NP7; 8V51 for D1-HLA-B*3501-NP10. No MTA is required. All other data needed to support the conclusions of the paper are present in the paper or the Supplementary Materials in the 'Data File s1' file.

FIGURE LEGENDS

Figure 1. Differential cross-reactivity of polyclonal CD8$^+$ T cells towards B*35:01/NP$_{418}$ variants. PBMCs from HLA-B*35:01$^+$ healthy donors were stimulated with a pool of 12 NP$_{418}$ peptide variants (Table 1) and expanded *in vitro* for 11 days. (**A**) NP$_{418}$ variants, and the respective names of HLA-B*35:01/NP$_{418}$ tetramers, are listed; (**B**) Representative flow cytometry dot plots of HLA-B*35:01/NP$_{418}$ tetramer$^+$ CD8$^+$ T cells, specific for the indicated NP$_{418}$ peptide variant. Frequency of CD3$^+$CD4$^-$CD8$^+$ B*35:01/NP$_{418}$ tetramer$^+$ cells are depicted. (**C**) Mean frequency (red lines) of B*35:01/NP$_{418}$-specific CD8$^+$ T cells reactive to

specific NP_{418} peptide variants across 3 different donors (d1, d2, d3). (**D**) Flow cytometry of $CD8^+$ T cells co-stained with B*35:01/NP_{418} tetramers conjugated with SAV-PE and SAV-BV421. Full panel shown in fig. S2. Frequency of cross-reactive HLA-B*35:01/NP_{418}^+ $CD8^+$ T cells across 3 donors are shown. (**E**) Mean frequency of cross-reactive B*35:01/NP_{418}-$CD8^+$ T cells (red lines) spanning the plausible co-staining combinations across 10 B*35:01/NP_{418} tetramers (as defined in (**A**). Each symbol represents an individual donor as denoted in (**C**). (**F**) Heat map depicting the frequencies of cross-reactive HLA-B*35:01/$NP_{418}^+CD8^+$ T cells across each B*35:01^+ donor (top) analysed as in (**E**) for a matrix of unique NP_{418} variant combinations (left). Bottom bar depicts the scale of gradient frequencies. Data are representative of n=3 donors. Experiments were reproduced for 5 additional donors, depicted in Figure 4. (**D**) d2 cells had lower cell numbers to start with, thus there are less cells displayed on the FACS plots. Viability was consistent between the donors. Dead cells were excluded from analysis.

Figure 2. The breadth and landscape of B*35:01/NP_{418} cross-recognition varies across different TCRs. To understand cross-recognition of B*35:01/NP_{418} variants at a single TCR$\alpha\beta$ level, J76 cell lines expressing a single B*35:01/NP_{418}-specific TCR$\alpha\beta$ were generated. (**A**) Gating strategy on J76 cells transduced with CD8α and HLA-B*35:01/NP_{418}-specific TCR$\alpha\beta$ encoding vectors is shown. (**B**) Representative CD69 expression staining (for the TCR.3180 clone) following 2hrs in TCR- and non-TCR-mediated stimulation is indicated across different stimulation conditions. (**C**) CD69 expression of HLA-B*35:01-restricted NP_{418}-specific TCR$\alpha\beta$-expressing J76 cell lines after stimulation with C1R-B*35:01 cells pulsed with NP_{418} peptide variants. (**D**) CD69 expression was quantified as Mean Fluorescence Intensity (MFI, arbitrary units, AU). Nil=no peptide; B35-IPS= irrelevant B*35:01-restricted CMV epitope (negative control); Pool (grey bars) refers to stimulation with 12 NP_{418} peptide variants. Data in (**C**) are representative of a minimum of n=3 independent experiments. Data in (**D**) represent the mean of n=3 replicate samples; error bars=SD. ***P<0.001 (one-way ANOVA followed by Tukey post-test comparing pooled to single peptides stimulations). Data are representative of n=2 independent experiments with similar results.

Figure 3. Functional avidity and antigen sensitivity of single HLA-B35:01/NP_{418}-specific TCR$\alpha\beta$. (**A**) Kinetic peptide-dose functional responses were measured as CD69 MFI expression in J76 cells transduced with HLA-B*35:01-restricted NP_{418}-specific TCRs (gated on $CD8^+$, $CD3^+$, GFP^+) stimulated overnight with varying concentrations of NP_{418} peptides presented by HLA-B*35:01^+ C1Rs. (**B**) Half maximal effective concentration (EC_{50}) was

determined as described in (**A**). Red-dotted lines represent area of 50% inhibition of CD69 expression. Data are representative of n=2 independent experiments with similar results.

Figure 4. CD8β co-receptor binding dependence of cross-reactive HLA-B*35:01-$NP_{418}$$^{+}$CD8^{+} T cell responses. PBMCs from HLA-B*35:01^{+} healthy donors were stimulated with a pool of 12 NP_{418} peptide variants (Table 1) and expanded *in vitro* for 11 days before dual PE- and BV421-tetramer staining sets of WT and CD8-NULL (table S2) tetramers. (**A**) Representative profiles of dual B*35:01/NP_{418}-PE and B*35:01/NP_{418}-BV421 tetramer staining using WT and NULL tetramers from d6. (**B**) Paired frequencies of cross-reactive HLA-B*35:01/NP_{418}-specific CD8^{+} T cells between WT (black) and NULL (grey) tetramer groups. (**C**) Mean frequency CD8 co-receptor dependence of cross-reactive HLA-B*35:01/NP_{418}-specific CD8^{+} T cells (n=5). Experiments were performed on 5 buffy pack donors (d4-8) from two independent experiments. Frequencies gated on live CD3^{+}CD8^{+} T cells.

Figure 5. Arginine at position five acts as a pivot for HLA-B*35:01/NP_{418} recognition despite distinct TCRαβ landscapes. (**A-D**). Activation of HLA-B*35:01-restricted NP_{418}-specific J76 cell lines stimulated with NP4 APLs carrying single alanine substitutions at positions 1, 4, 5, 6, 7 and 8 presented by HLA-B*35:01^{+} C1R cells. Representing the mean of n=3 replicates samples; error bars=SD. ***P<0.001 (one-way ANOVA followed by Tukey post-test comparing NP4 'wt' to ALPs. Representative of n=2 independent experiments with similar results. (**E**) HLA-B*35:01(cartoon) and NP_{418} (stick representation) binary structure with residues labelled.

Figure 6. Cytokine and polyfunctional profiles of primary HLA-B*35:01/NP_{418}-specific CD8^{+} T cell clones. (**A**) IFN-γ production of primary CD8^{+} T cell clones D1 and 3180 following 5hr stimulation with HLA-B*35:01^{+} C1Rs and analysed by ICS. (**B**) Representative flow cytometry data of cytokine production (IFN-γ, TNF, MIP-1β) and CD107a expression (gated on live, CD3^{+}CD8^{+} cells). (**C**) Polyfunctional profiles (IFN-γ, TNF, MIP-1β) primary clones D1 and 3180 (left) among cytokine-positive or CD107a-positive cells. (**A**) Avidity EC50 values are representative of n=3 independent experiments with similar results and cytotoxicity EC50, as previously described. (**A-C**) Representative of n=1 experiment.

Figure 7. Structural cross-recognition of the HLA-B*35:01/NP_{418} epitope.

Cartoon representation of the 3180 TCR (**A**) with α-chain in orange, and β-chain in green recognizing NP7 variant (dark grey sticks) presented by HLA-B*35:01. The HLA-B*35:01 chain is colored white. The CDR1α, CDR2α, CDR3α loops are shown in red, pink and cyan, while

the CDR1β, CDR2β, and CDR3β loops are shown in yellow, blue, and purple, respectively. (**B**) The left panel show the atomic footprint of the 3180 TCR on the surface of HLA-B*35:01 presenting NP7. The corresponding TCR segments involved in contact are coloured according to the prior panel, framework contacts are coloured in green; the center-of-mass for the Vα and Vβ are shown. On the right, the pie charts represent the % contribution of each 3180 TCR segment towards the total binding. (**C**) 3180 TCR contacts with the NP7 peptide using a stick representation with TCR. Equivalent representations for the D1 TCR with the NP7 peptide (**D-F**).

Table 1. Variation in HLA-B*35:01-restricted $NP_{418-426}$ epitope.

Sequence	Variable motif[a]	Code	Year(s)	Virus(es)
LPF**DRP**T**I**M	DRP/I	NP1	1933	H1N1
LPF**DRT**T**I**M	DRT/I	NP2	1934	H1N1
LPF**DKP**T**I**M	DKP/I	NP3	1957/1968	pH2N2-1957; pH3N2-1968
LPF**DKS**T**I**M	DKS/I	NP4	1972	H3N2
LPF**DKT**T**I**M	DKT/I	NP5	1947	H1N1; H2N2
LPF**DKS**T**V**M	DKS/V	NP6	1977	H1N1; H3N1
LPF**EKS**T**I**M	EKS/I	NP7	2002	H3N2
LPF**DKA**T**I**M	DKA/I	NP8	2005	H1N1
LPF**DIA**T**I**M	DIA/I	NP9	2006	H1N1
LPF**EKS**T**V**M	EKS/V	NP10	1980	H3N2
LPF**ERA**T**V**M	ERA/V	NP11	2009	pH1N1-2009
LPF**ERA**T**I**M	ERA/I	NP12	1918/1997/2014/2024	pH1N1-1918; H5N1-1997; H7N9-2014; H5N1-2024[b]

Bold and underlined indicate variable residues.
[a]Residues 4, 5, 6 and 8 in NP_{418} constitute the variable motif.
[b]Sequences from 2024 H5N1bovine and avian influenza outbreak.

Table 2. TCRs of HLA-B*3501-NP$_{418}$-specific CD8$^+$ T cell clones.

Clone	TCR chain	V – CDR3 loop – J	Variants recognized (in blue)	Length (aa)	Count (pairs)
D1	α	TRAV1*01 TRAJ9*01 tgcgccgtggatactggaggcttcaaaactatctttt C A V D T G G F K T I F	NP3$^-$ NP4$^-$ NP5$^-$	7	27
	β	TRBV7-8*01 TRBJ2-5.1 tgtgccagcagcccacaggggccaggagacccagtacttc C A S S P T G G Q E T Q Y F	**NP10$^+$**	9	
2384	α	TRAV8.1*01 J_α18*01 tgtgccgtgaatgctggaggctcaaccctggggaggctatacttt C A V N A G G S T L G R L Y F	NP3$^-$ **NP4$^+$** **NP5$^+$**	10	54
	β	TRBV20-1*01 TRBJ2-5.1 tgtagtgctggtgggcagggcatccaccaagagacccagtacttc C S A G G Q G I H Q E T Q Y F	NP10$^-$	10	
C4	α	TRAV2*01 TRAJ33*01 tgtgctgtggaggggtatagcaactatcagttaatctgg C A V E G Y S N Y Q L I W	**NP3$^+$** **NP4$^+$** **NP5$^+$**	8	12
	β	TRBV 4-2*01 TRBJ1-2 tgtgctagcagccccgaccctacaggggatgcggactatggctacaccttc C A S S P D P T G D A D Y G Y T F	NP10$^-$	9	
3180	α	TRAV13-1 TRAJ28*01 tgtgcagcagacgggggggctgggagttaccaactcactttc C A A D G G A G S Y Q L T F	**NP3$^+$** **NP4$^+$** **NP5$^+$**	8	9
	β	TRBV20-1*02 TRBJ2-3*01 tgtagtgctggtcccactagcggtcgcacagatacgcagtatttt C S A G P T S G R T D T Q Y F	**NP10$^+$**	9	

Paired TCRαβ sequences from single cell-sorted CD3$^+$ CD8$^+$ cells, isolated from *in vitro*-expanded HLA-B35*01-NP$_{418}$-specific T cell clones. Amino acid (upper case) and nucleotide (lower case) sequences coding for V-regions (dark grey) and J-regions (light grey). Boxed areas show non-germline, N-encoded TCRα and N-D$_\beta$-N encoded TCRβ nucleotides. Phenotype, number of NP$_{418}$ variants recognized as previously assessed(*27*). aa, amino acid. Count, number of TCRαβ paired sequences per clone. Underlined residues directly contact the NP epitopes.

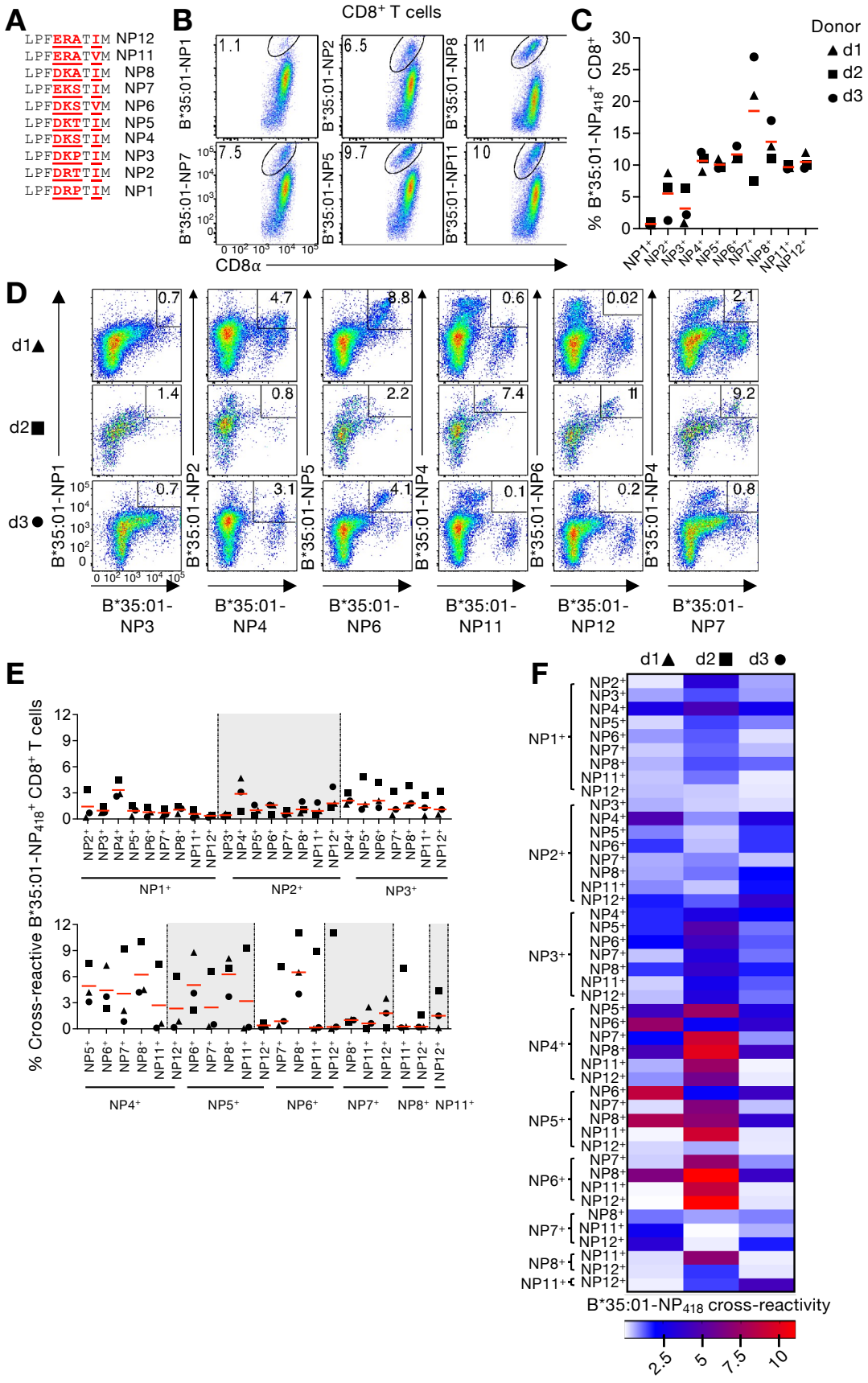

Fig. 1 Quiñones-Parra *et al*

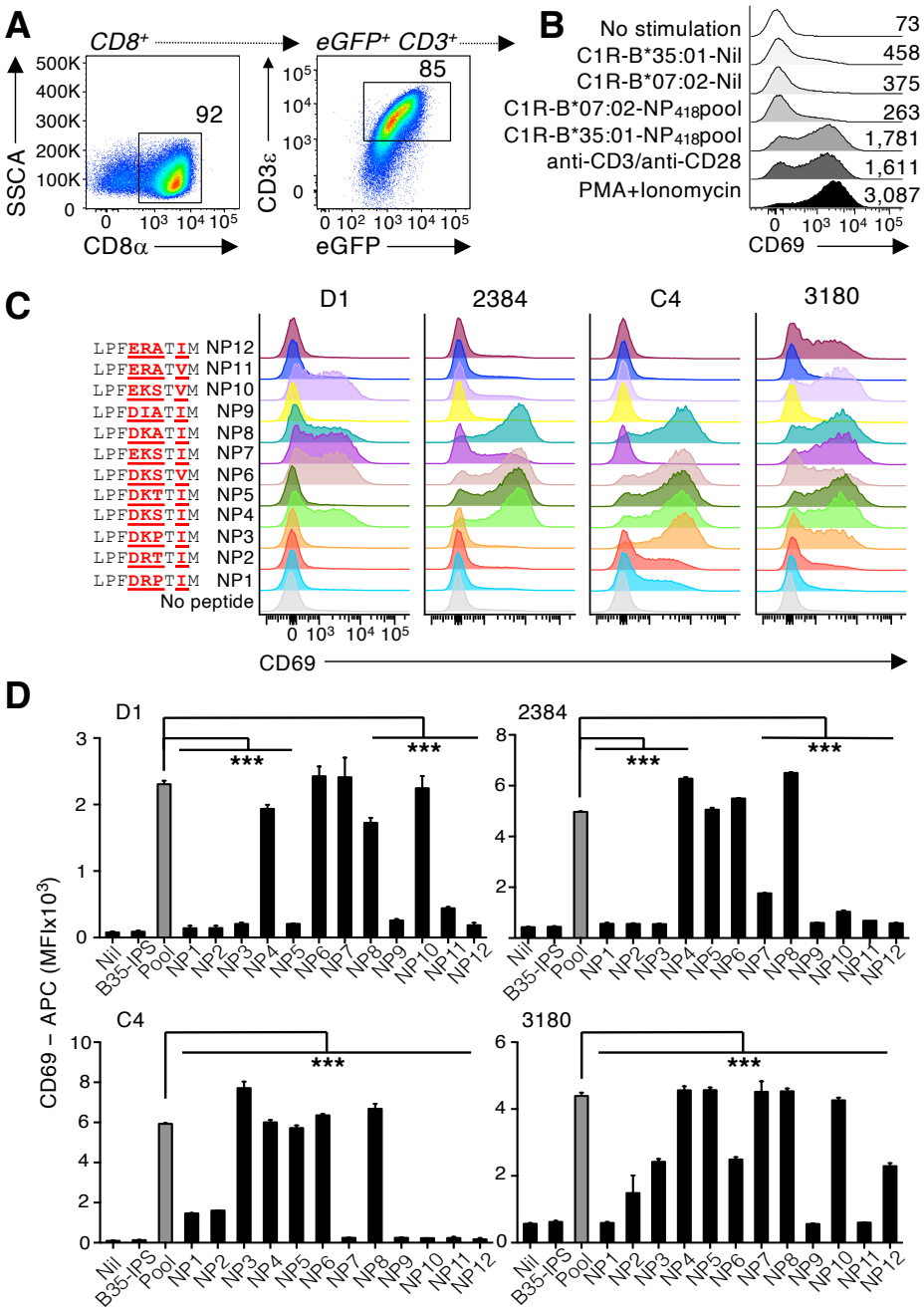

Fig. 2 Quiñones-Parra *et al*

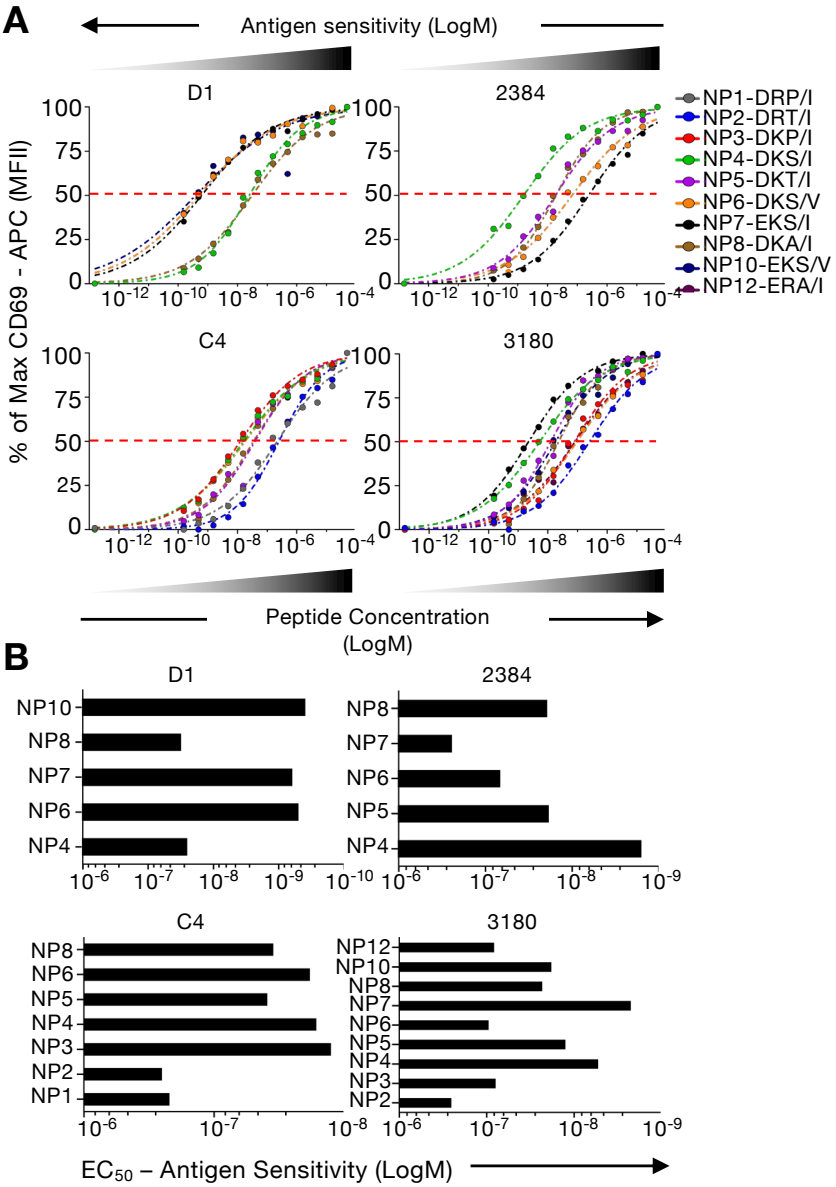

Fig. 3 Quiñones-Parra *et al*

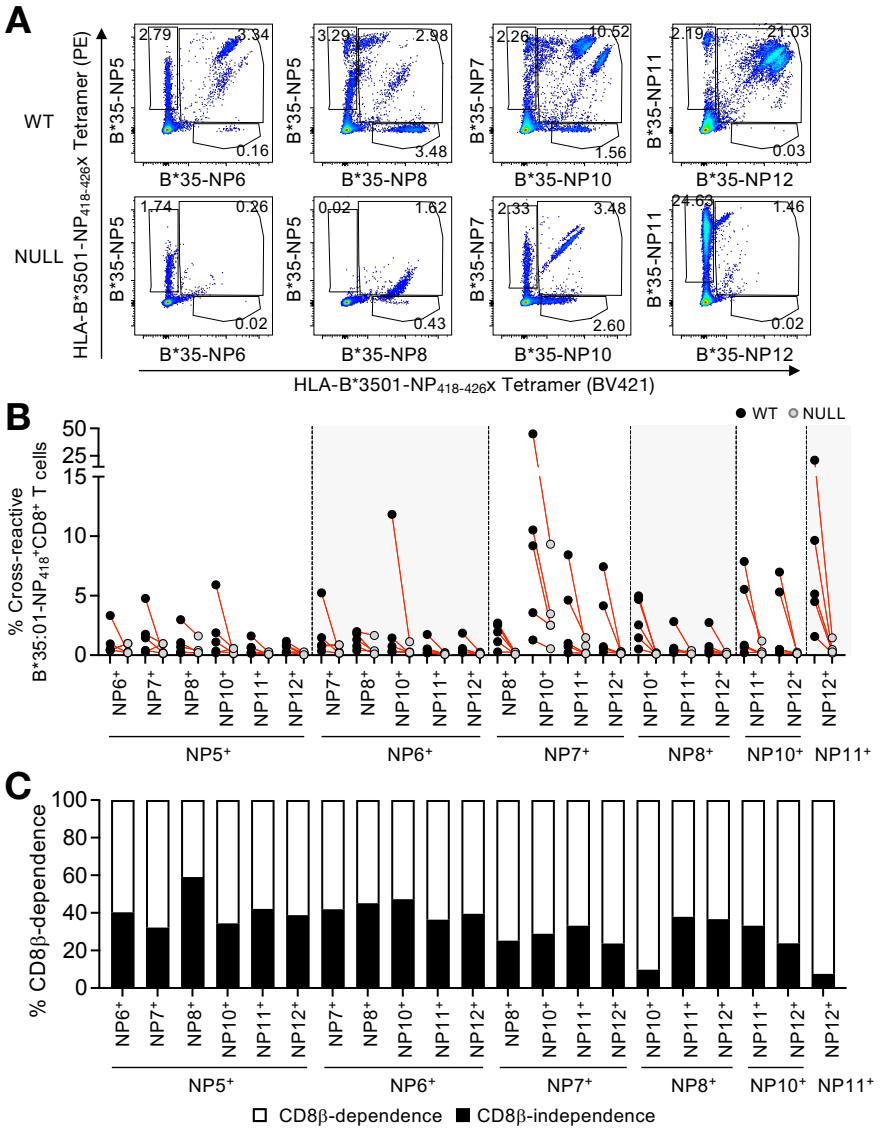

Fig. 4 Quiñones-Parra *et al*

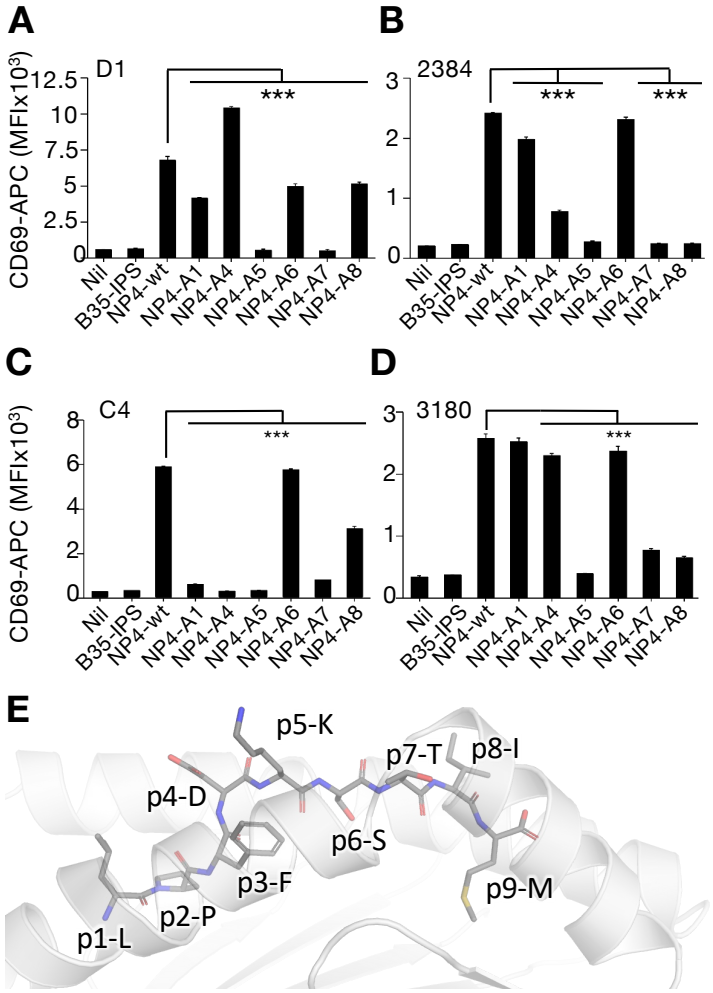

Fig. 5 Quiñones-Parra *et al*

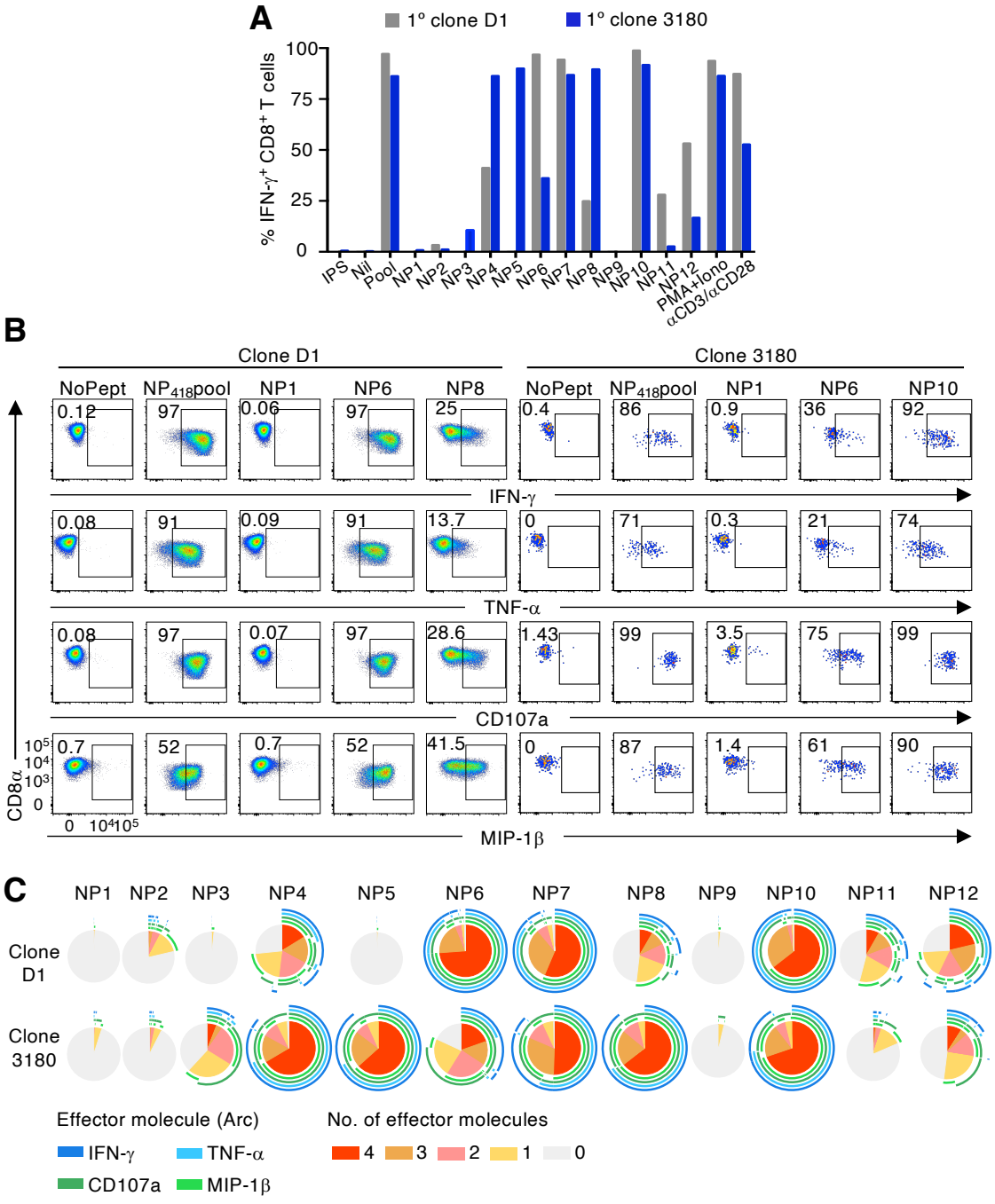

Fig. 6 Quiñones-Parra et al

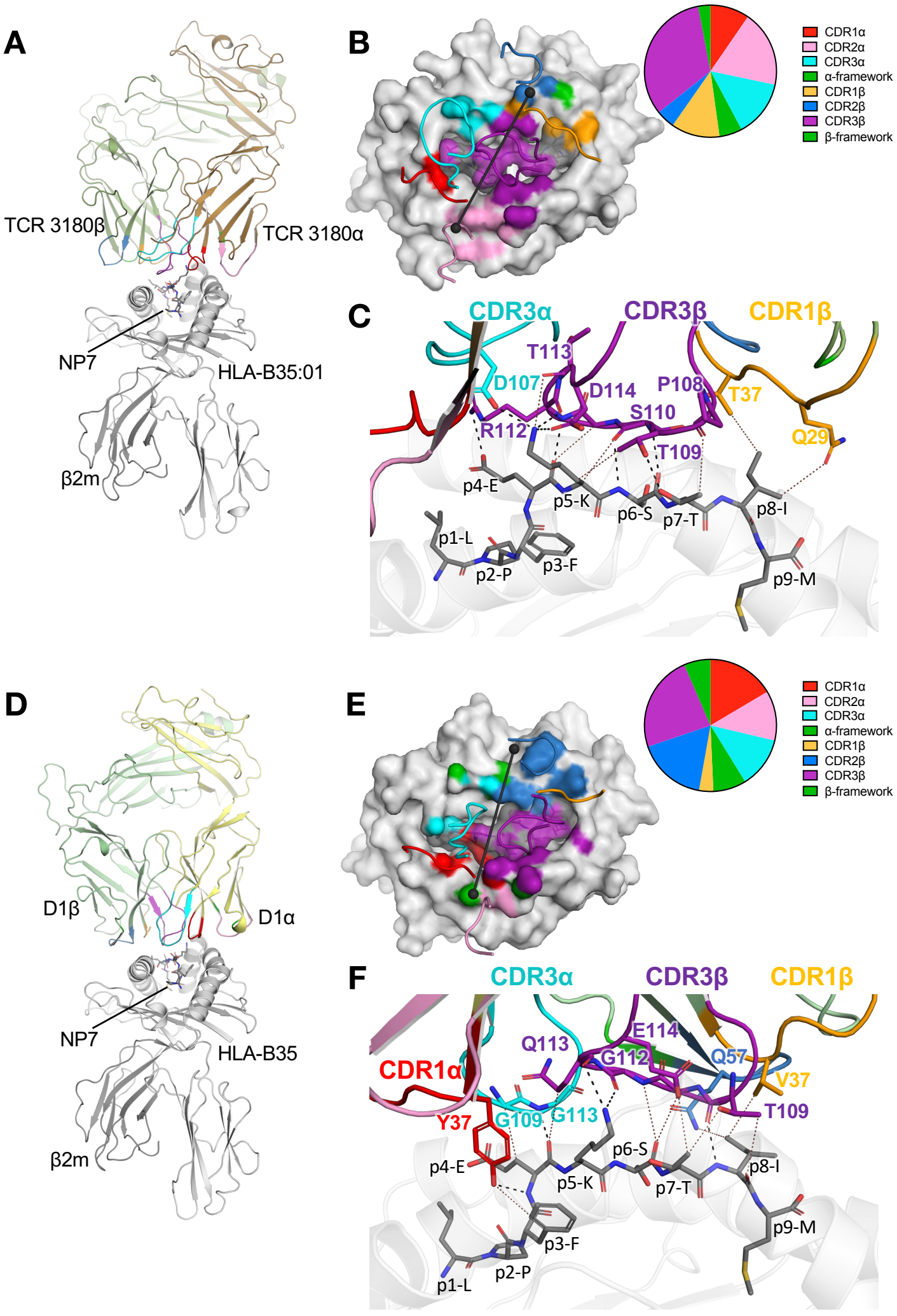

Fig. 7 Quiñones-Parra *et al*

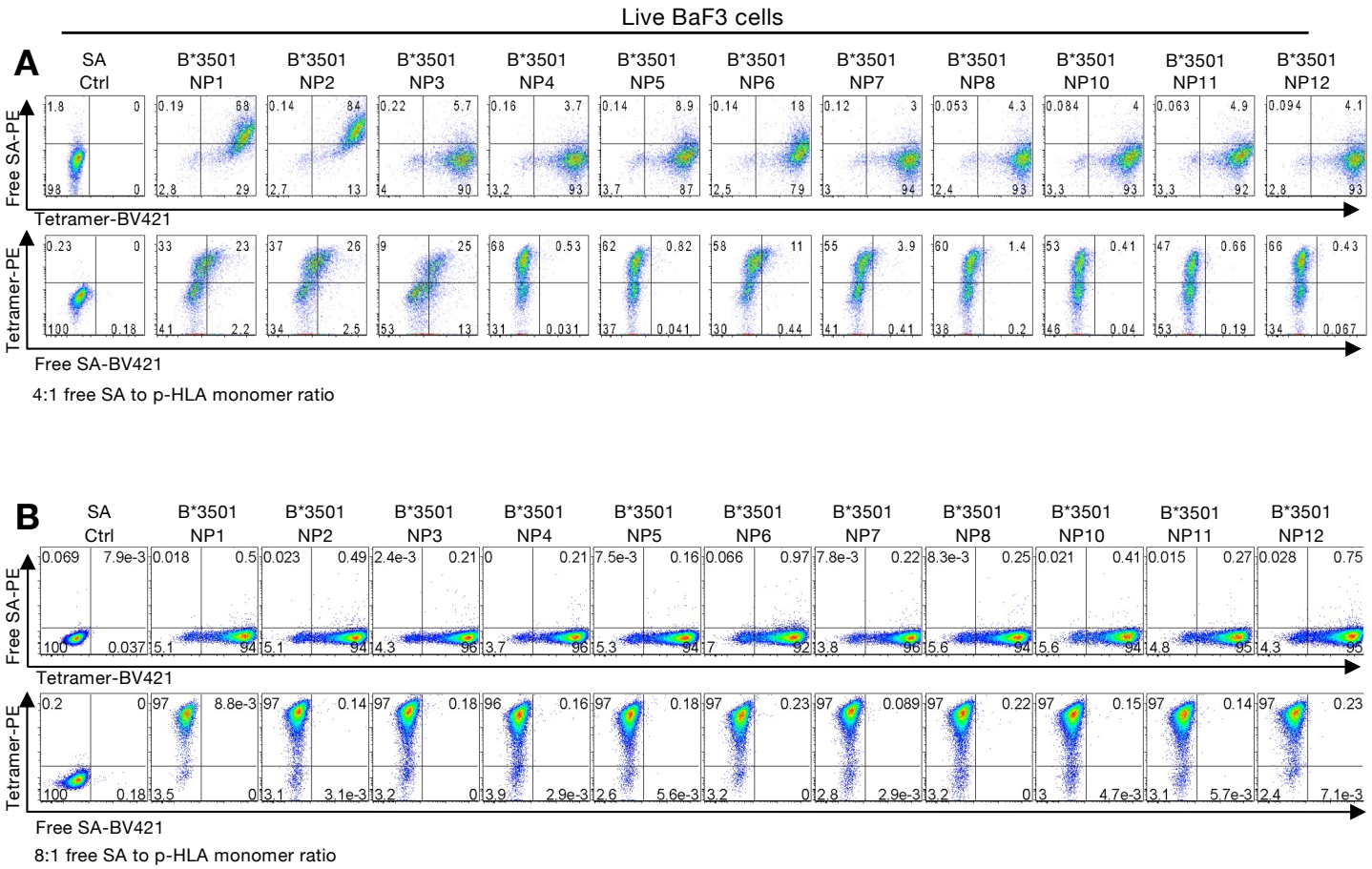

Fig. S1. LILRB1-expressing Ba/F3 cells stained with B*35:01-NP$_{418}$-PE or B*35:01-NP$_{418}$-BV421. (**A, B**) Staining with tetramers conjugated with SA-PE in the presence of equivalent amounts of 'free' SA-BV421 and the converse was performed. Staining with tetramers conjugated with BV-421 was performed in the presence free-SA-PE. **(A)** Flow cytometry profiles with B*35:01-NP$_{418}$ tetramers conjugated at 4:1 free SA to p-HLA monomer ratio; and **(B)** FACS profiles B*35:01/NP$_{418}$ tetramers conjugated at 8:1 free SA to p-HLA monomer ratio. Related to Fig. 1.

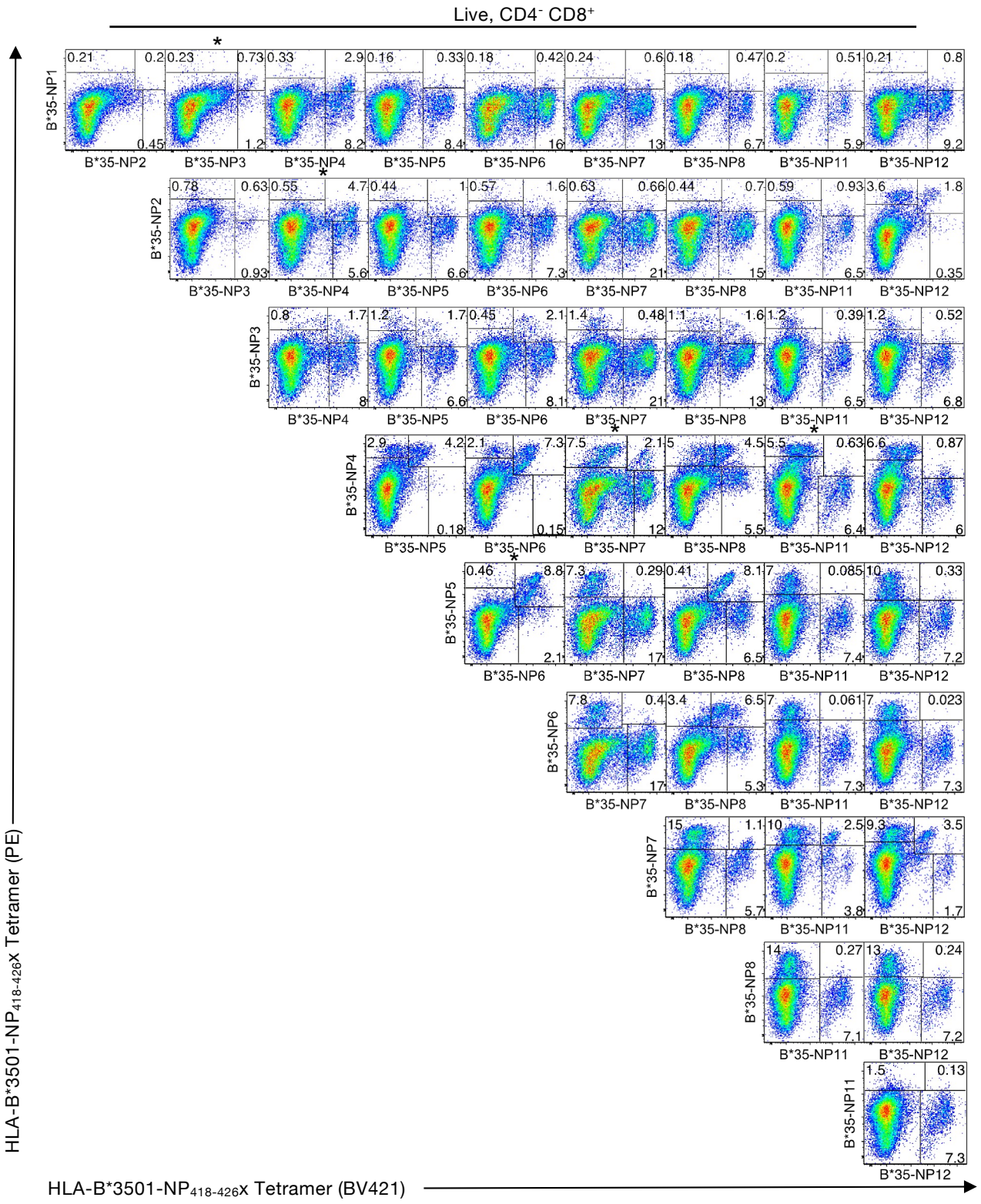

Fig. S2. Flow cytometry profiles of distinct dual B*35:01/NP_{418}-PE and B*35:01-NP_{418}-BV421 tetramer staining for a representative d1 donor. FACS plots with asterisk (*) above are also presented in Figure 1D. Related to Fig. 1.

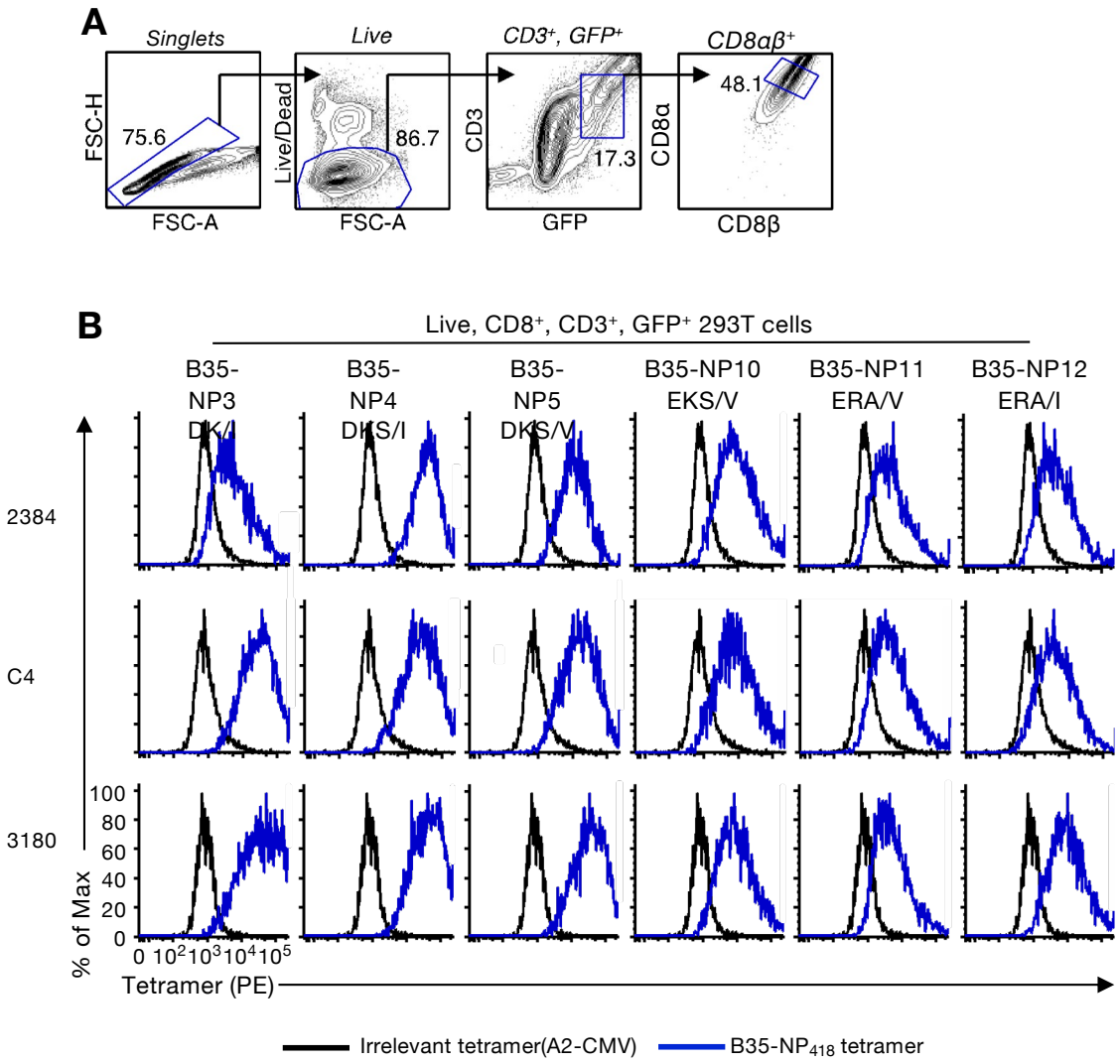

Fig. S3. Validation of B*35:01/NP$_{418}$-tetramer and confirmation of TCR reactivity. 293T cells were transfected with pMIGII plasmids encoding CD3-GFP, CD8 and B*35:01/NP$_{418}$-specific TCRs-GFP (2384, C4 and 3180) and TCR expression and specificity was verified 48h after transfection by HLA-B35:01/NP$_{418}$ tetramer staining. (**A**) Gating strategy for analysis of live, CD3$^+$, GFP$^+$, CD8αβ$^+$ 293T cells; (**B**) Ability of transfected 293T cells to bind B*35:01/NP$_{418}$ tetramers specific for a panel of peptide variants (top). An irrelevant A*0201-NLV (CMV-specific) tetramer was used to determine the level of background tetramer staining. Related to Fig. 2.

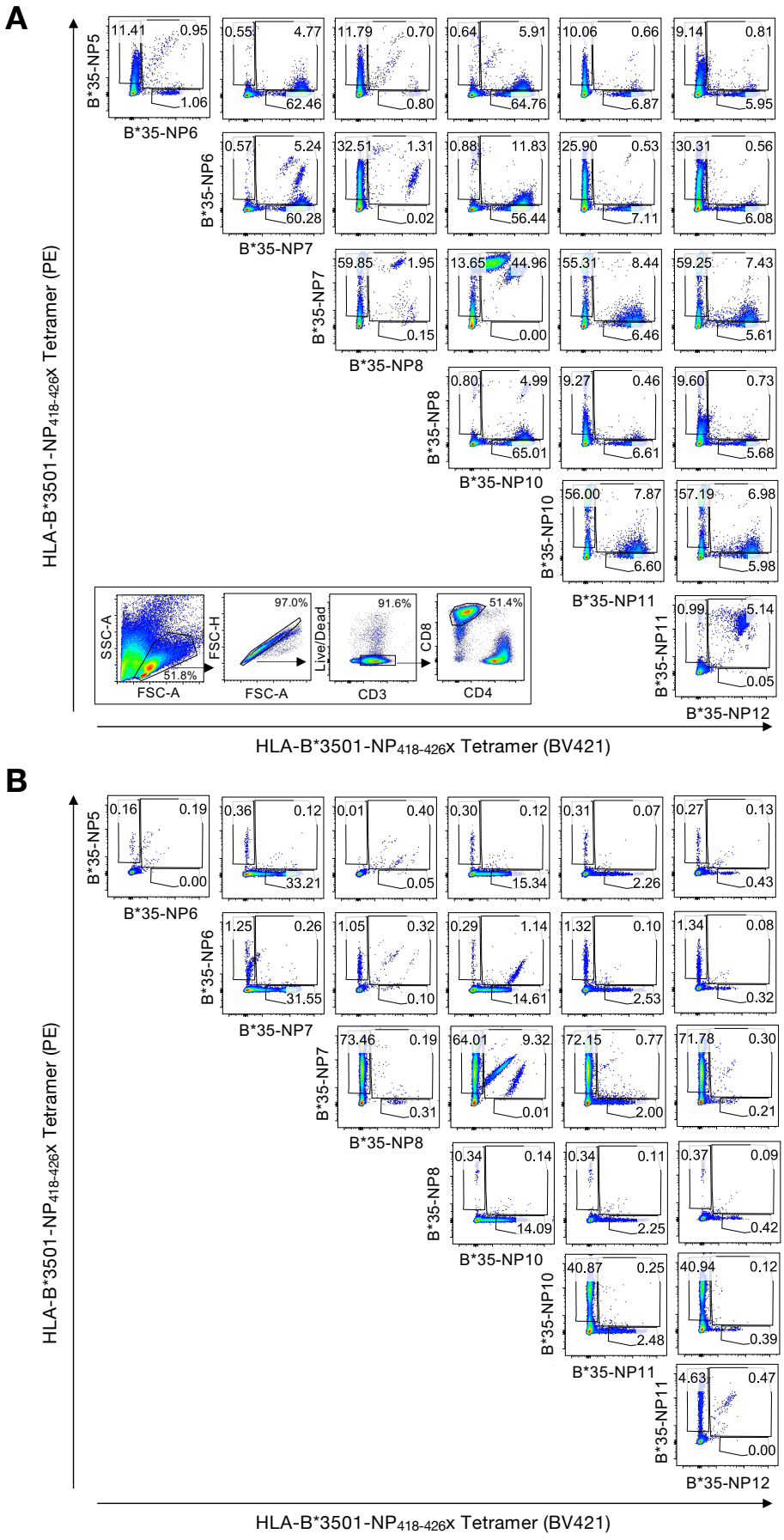

Fig. S4. Flow cytometry profiles of dual B*35:01/NP$_{418}$-PE and B*35:01-NP$_{418}$-BV421 tetramer staining using WT and NULL tetramers. Representative profiles of WT (**A**) and NULL (**B**) tetramer staining from d5. Experiments were performed on 5 buffy pack donors (d4-8) in two independent experiments. Frequencies gated on live CD3^{+}CD8^{+} T cell cultures; strategy shown in bottom left inset of (**A**). Related to Fig. 4.

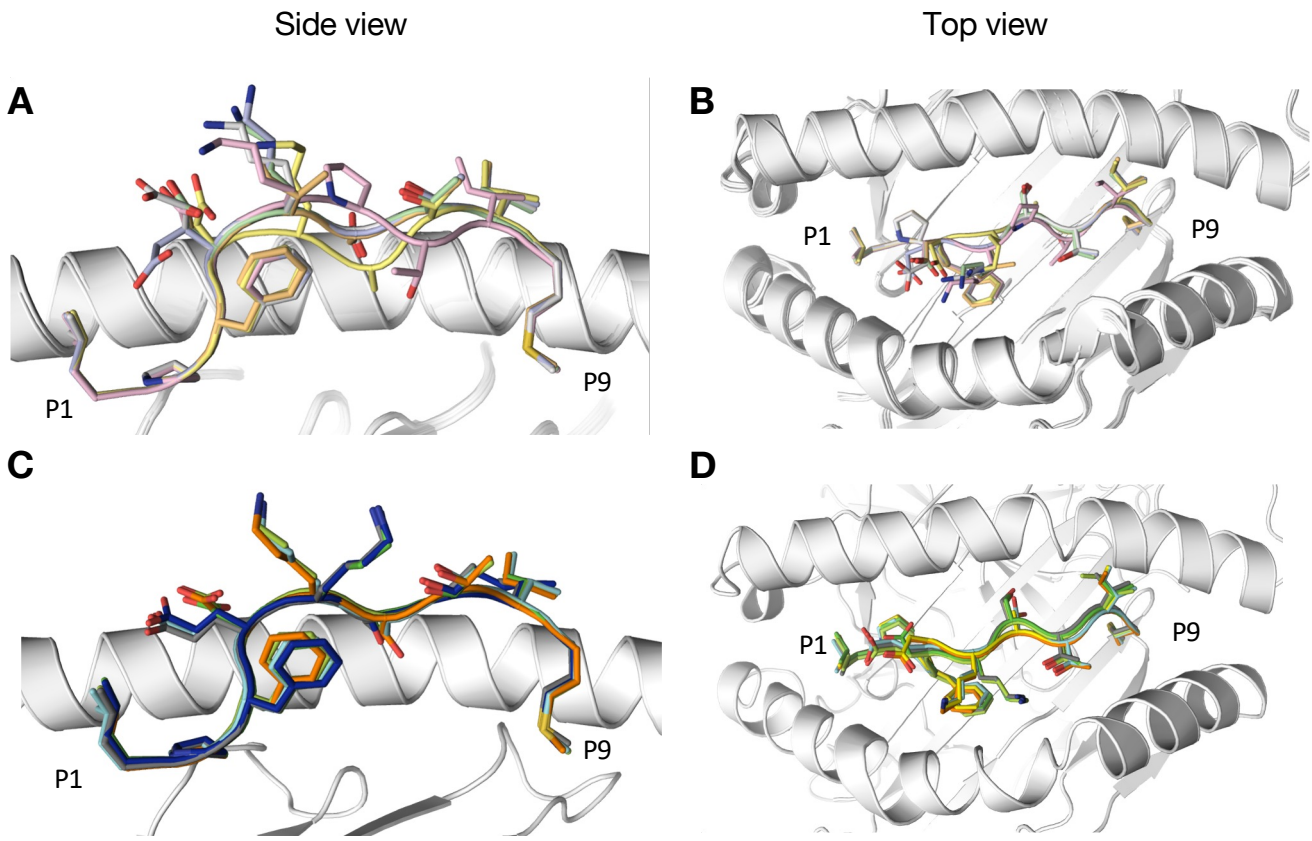

Fig. S5. HLA-B*35:01-NP$_{418}$ variant structures. (A-B) Overlay of the HLA-B*35:01 complexed to NP$_{418}$ peptide variants: in light pink NP3, in pale green, NP6, in light blue, NP7, in yellow NP8, and in orange NP9. The structures are aligned to the LPFEKSTVM/HLA-B*35:01 structure as reference (pdb : 3LKS). The peptides are shown in ribbon and sticks whereas the MHC is shown in cartoon representation. (**A**) side view and (**B**) top view of the binding cleft. (**C-D**) Overlay of the HLA-B*35:01 presenting NP$_{418}$ peptide variants upon D1 or 3180 TCR binding: in green D1-NP6, in blue D1-NP7, cyan 3180-NP7, in limon 3180-NP8, and in orange D1-NP10. The structures are aligned to the LPFEKSTVM/HLA-B*35:01 structure as reference (pdb: 3LKS). The peptides are shown in ribbon and sticks whereas the MHC is shown in cartoon representation. (**C**) side view and (**D**) top view. Related to Fig. 7.

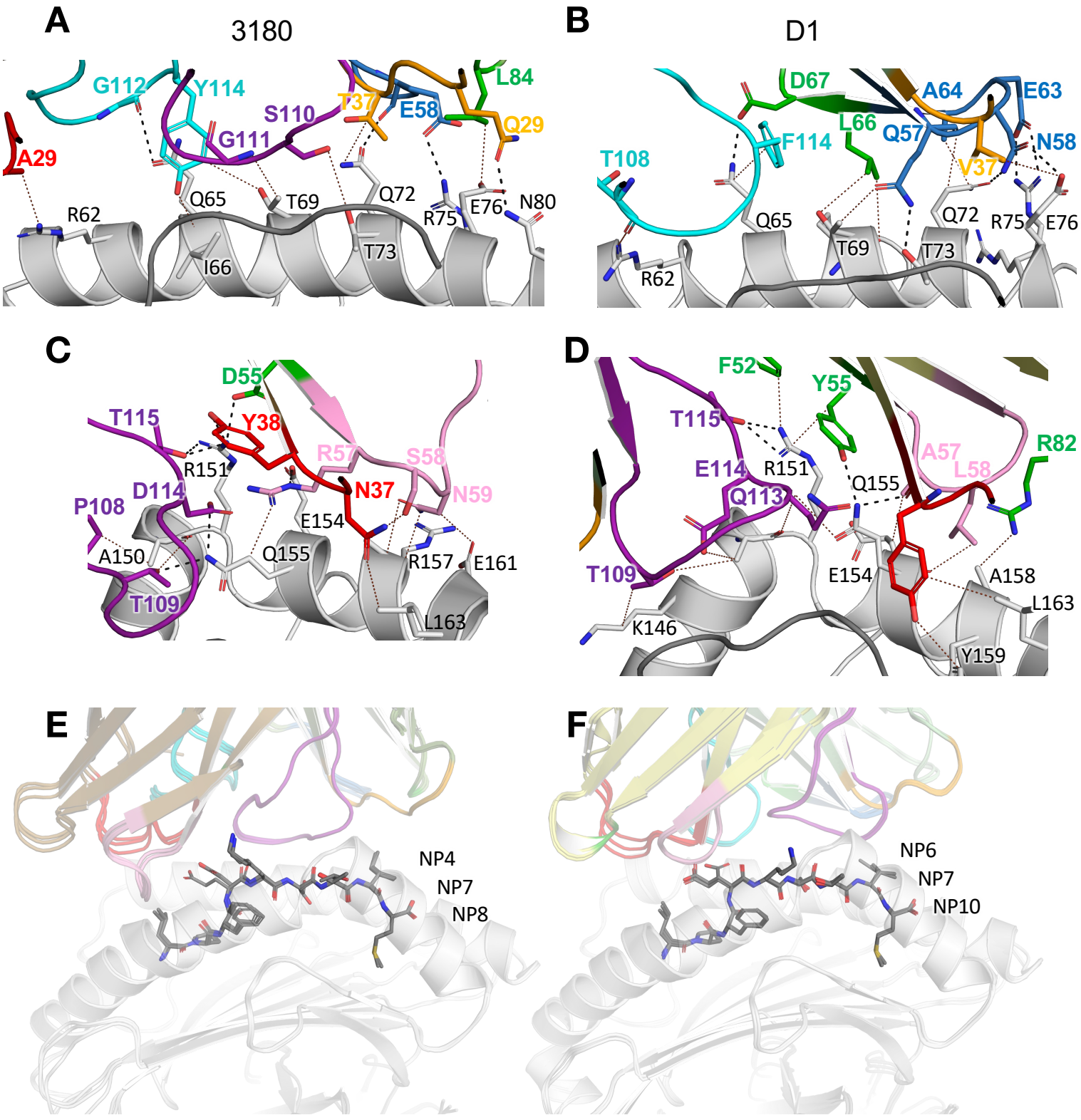

Fig. S6. 3180 and D1 ternary structures. CDR loop interactions with the HLA-B*35:01 α1 helix upon (**A**) 3180 TCR binding or (**B**) D1 TCR binding. (**C, D**) equivalent interactions for the α2 helix. (**E**) Overlayed 3180-bound structures for the solved NP_{418} viral variant peptides and (**F**) the corresponding overlay for the D1-bound structures. Related to Fig. 7.

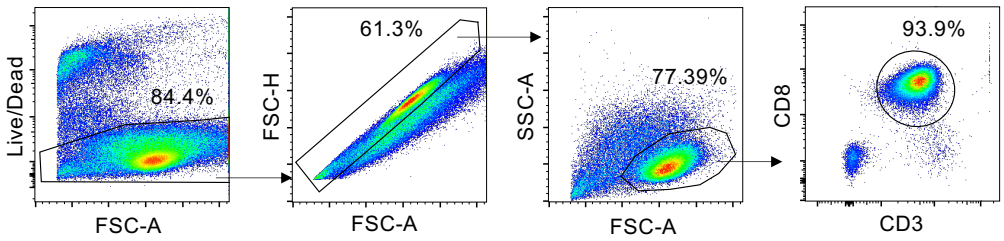

Fig. S7. Gating strategy for primary T cell clones. Representative D1 T cell clone is shown. Related to Fig. 6.

Table S1. Surface Plasmon Resonance: affinity measurements of 3180 and D1 TCRs.

Sequence	Name	Year	Virus	TCR Recognition	
				3180 TCR (Kd)	D1 TCR (Kd)
LPFDRPTIM	NP1	<1933	hH1N1-WSN-1933	NB	NB
LPFDRTTIM	NP2	1934	hH1N1-PR8-1934	NB	NB
LPFDKPTIM	NP3	1957	pH2N2-1957/pH3N2-1968	58.3 ± 1.4* (N=2)	NB
LPFDKSTIM	NP4	1972	H3N2-Udorn-1972	12.3 ± 1.5 (N=2)	NB
LPFDKTTIM	NP5	1947	H1N1-1983/sH1N1-Solomon-2006	14.5 ± 1.0 (N=2)	NB
LPFDKSTVM	NP6	1977	H1N1/H3N2	99.5 ± 3.4 (N=2)	> 200 (N=1)
LPFEKSTIM	NP7	2002	sH3N2-Brisb	11.4 ± 1.0 (N=1)	109.1 ± 10.8 (N=1)
LPFDKATIM	NP8	2005	H1N1	10.9 ± 1.3 (N=2)	NB
LPFDIATIM	NP9	2006	H1N1	NB	NB
LPFEKSTVM	NP10	1980	H3N2	37.7 ± 1.8 (N=1)	38.0 ± 3.0 (N=1)
LPFERATVM	NP11	2009	pH1N1-09-(Auck09)	NT	NT
LPFERATIM	NP12	1918	H7N9/pH1N1-1918/H5N1	78.3 ± 2.3 (N=2)	NB

Kd is in μM; NB: no binding at maximum concentration of analyte tested of 200 μM; NT: not tested. N=number of independent experiments performed.

*The error is representative of the standard deviation of the experiment performed in duplicate.

All independent experiments were performed with the NP4 peptide as positive control, and in duplicate.

Table S2. HLA-B*35:01-NP_{418} CD8-null tetramers generated for the assessment of cross-reactive responses independent of CD8β co-receptor binding.

Monomer	Amino acid sequence
IAV_B35_NP_{418}_NP5-CD8 null	LPFDKTTIM
IAV_B35_NP_{418}_NP6-CD8 null	LPFDKSTVM
IAV_B35_NP_{418}_NP7-CD8 null	LPFEKSTIM
IAV_B35_NP_{418}_NP8-CD8 null	LPFDKATIM
IAV_B35_NP_{418}_NP10-CD8 null	LPFEKSTVM
IAV_B35_NP_{418}_NP11-CD8 null	LPFERATVM
IAV_B35_NP_{418}_NP12-CD8 null	LPFERATIM

HLA-B*35:01-NP_{418} NP5 (LPFDKTTIM), HLA-B*35:01-NP_{418} NP6 (LPFDKSTVM), HLA-B*35:01-NP_{418} NP7 (LPFEKSTIM), HLA-B*35:01-NP_{418} NP8 (LPFDKATIM), HLA-B*35:01-NP_{418} NP10 (LPFEKSTVM), HLA-B*35:01-NP_{418} NP11 (LPFERATVM) and HLA-B*35:01-NP_{418} NP12 (LPFERATIM).

Table S3. Data collection and refinement statistics for the peptide-MHC structures.

	HLA-B*3501-NP3	HLA-B*3501-NP6	HLA-B*3501-NP7	HLA-B*3501-NP8	HLA-B*3501-NP9
Resolution range (Å)	33.84 – 1.67 (1.73 – 1.67)	25.9 – 1.81 (1.87 – 1.81)	26.51 – 1.83 (1.90 – 1.83)	37.23 – 1.57 (1.63 – 1.57)	24.80 – 1.75 (1.81 – 1.75)
Space group	$P\,2_1\,2_1\,2_1$	$P\,2_1\,2_1\,2_1$	$P\,2_1\,2_1\,2_1$	$P\,2_1\,2_1\,2_1$	$P\,2_1\,2_1\,2_1$
Unit cell (Å)	50.82 81.52 109.14	51 81.65 109.24	51.17 81.93 110.39	50.87 81.53 109.26	50.92 81.74 109.42
Total reflections	106742 (10525)	85106 (8118)	83116 (7995)	126534 (12248)	93427 (9066)
Unique reflections	53407 (5266)	42596 (4086)	41590 (4007)	63452 (6187)	46767 (4567)
Multiplicity	2.0 (2.0)	2.0 (2.0)	2.0 (2.0)	2.0 (2.0)	2.0 (2.0)
Completeness (%)	1.00 (1.00)	1.00 (0.97)	1.00 (0.98)	0.99 (0.98)	1.00 (0.99)
Mean I/sigma(I)	17.46 (3.61)	19.60 (3.43)	15.70 (4.39)	20.85 (2.82)	17.81 (3.50)
Wilson B-factor	16.38	18.18	17.06	17.48	16.95
R-merge	0.02453 (0.2076)	0.02641 (0.2191)	0.0295 (0.1698)	0.01904 (0.2785)	0.02969 (0.2304)
R-meas	0.0347 (0.2935)	0.03735 (0.3098)	0.04172 (0.2401)	0.02693 (0.3939)	0.04199 (0.3258)
CC1/2	0.999 (0.902)	0.999 (0.898)	0.998 (0.922)	1 (0.854)	0.999 (0.888)
R-work	0.1867 (0.2536)	0.1864 (0.2725)	0.1796 (0.2399)	0.1883 (0.2662)	0.1817 (0.2581)
R-free	0.2162 (0.2767)	0.2164 (0.2767)	0.2130 (0.2752)	0.2210 (0.2960)	0.2234 (0.2968)
RMS (bonds, Å)	0.014	0.010	0.010	0.014	0.014
RMS (angles, °)	1.60	1.60	1.58	1.62	1.64
Ramachandran favored (%)	98	98	99	98	99
Ramachandran allowed (%)	1.3	1.8	1	1.6	1
Ramachandran outliers (%)	0.26	0.26	0.26	0	0.26

Statistics for the highest-resolution shell are shown in parentheses.
PDB codes: 8EMK for HLA-B*3501-NP3; 8EMF for HLA-B*3501-NP6; 8EMG for HLA-B*3501-NP7; 8EMI for HLA-B*3501-NP8; 8EMJ for HLA-B*3501-NP9.

Table S4. Data collection and refinement statistics for the TCR-complex structures.

	3180-HLA-B*3501-NP4	3180-HLA-B*3501-NP7	3180-HLA-B*3501-NP8	D1-HLA-B*3501-NP6	D1-HLA-B*3501-NP7	D1-HLA-B*3501-NP10
Resolution range (Å)	27.0-2.70 (2.80-2.70)	49.47-2.50 (2.59-2.50)	48.95-2.30 (2.38-2.30)	38.59-2.65 (2.75-2.65)	46.72-2.40 (2.49-2.40)	39.5-2.10 (2.18-2.10)
Space group	$P\,2_1\,2_1\,2_1$	P 2_1	P 2_1	$P\,2_1\,2_1\,2_1$	$P\,2_1\,2_1\,2_1$	I 2
Unit cell (Å)	79.77 116.686 253.184	168.15 79.55 172.19 β = 95.56°	168.088 79.468 172.173 β = 95.53°	78.58 192.162 252.82	78.988 190.209 250.43	149.269 46.155 161.964 β = 101.4°
Total reflections	131468 (12936)	312868 (30013)	401920 (39893)	224005 (22146)	295899 (29146)	127751 (12561)
Unique reflections	65736 (6466)	156773 (15158)	201262 (20019)	112003 (11071)	147969 (14575)	63927 (6281)
Multiplicity	2.0 (2.0)	2.0 (2.0)	2.0 (2.0)	2.0 (2.0)	2.0 (2.0)	2.0 (2.0)
Completeness (%)	1.00 (1.00)	1.00 (0.97)	1.00 (1.00)	1.00 (1.00)	1.00 (1.00)	1.00 (1.00)
Mean I/sigma(I)	13.93 (1.97)	13.49 (2.68)	13.09 (2.88)	10.05 (2.47)	12.64 (2.06)	8.59 (2.39)
Wilson B-factor	46.09	41.33	33.64	34.95	36.35	30.40
R-merge	0.05087 (0.4143)	0.03737 (0.287)	0.03995 (0.2803)	0.05045 (0.2729)	0.04402 (0.3912)	0.03697 (0.2798)
R-meas	0.07195 (0.5859)	0.05286 (0.4059)	0.0565 (0.3964)	0.07134 (0.3859)	0.06225 (0.5533)	0.05228 (0.3957)
CC1/2	0.993 (0.702)	0.998 (0.811)	0.998 (0.817)	0.997 (0.87)	0.999 (0.784)	0.999 (0.8)
R-work	0.2207 (0.2856)	0.1985 (0.2595)	0.1917 (0.2485)	0.2288 (0.2870)	0.2529 (0.3310)	0.2262 (0.2743)
R-free	0.2514 (0.3450)	0.2393 (0.3022)	0.2307 (0.2905)	0.2636 (0.3197)	0.2656 (0.3347)	0.2495 (0.2885)
RMS (bonds, Å)	0.011	0.013	0.014	0.010	0.010	0.011
RMS (angles, °)	1.69	1.63	1.75	1.56	1.52	1.66
Ramachandran favored (%)	96	97	97	96	96	96
Ramachandran allowed (%)	4.2	2.9	3.3	4.3	4.3	4.1
Ramachandran outliers (%)	0.25	0.12	0.19	0.22	0.19	0.12

Statistics for the highest-resolution shell are shown in parentheses. PDB codes: 8EN8 for 3180-HLA-B*3501-NP4; 8ENH for 3180-HLA-B*3501-NP7; 8EO8 for 3180-HLA-B*3501-NP8; 8V50 for D1-HLA-B*3501-NP6; 8V4Z for D1-HLA-B*3501-NP7; 8V51 for D1-HLA-B*3501-NP10.

Table S5. Contribution to buried surface area of TCR: peptide-MHC complexes.

TCR	peptide	BSA	Vα	Vβ	peptide	1α	2α	3α	Fwα	1β	2β	3β	Fwβ	angle	sc
3180	NP4	1920	45.3	54.7	18.8	7.3	19.8	12.3	5.9	13.3	2.8	34.1	4.44	63	0.64
	NP7	2040	47.8	52.2	17.2	9.6	18.7	13.9	5.6	11.9	4.6	32.7	3.0	63	0.66
	NP8	19670	46.1	53.9	18.9	7.7	18.6	13.8	6.0	12.6	4.2	33.3	3.8	64	0.62
	average	1980	46.4	53.6	18.3	8.2	19.0	13.3	5.8	12.6	3.9	33.4	3.7	63	0.64
D1	NP6	1910	49.3	50.7	18.4	16.5	12.2	12.5	8.1	3.5	17.0	23.7	6.5	76	0.70
	NP7	1990	47.6	52.4	19.2	17.2	11.4	11.3	7.7	3.4	18.2	22.9	7.9	77	0.70
	NP10	2000	50.7	49.3	17.2	18.9	12.4	12.1	7.3	2.8	17.1	22.3	7.0	73	0.66
	average	1970	49.2	50.8	18.3	17.5	12.0	12.0	7.7	3.2	17.4	23.0	7.1	75	0.68
Literature	Average value	1910	52.0	47.5	28.9	16.0	11.6	20.3		7.2	11.9	23.9		63	0.65
	Smallest value	1240	33.0	22.0	17.0	3.5	5.1	4.6		0	0	8.3		37	0.41
	Largest value	2400	78.0	67.0	48.6	28.7	19.7	34.7		19.2	33.3	42		90	0.80

BSA: Buried Surface Area (Å2) total calculated with AreaIMol (CCP4), Vα: contribution of the α-chain to the TCR BSA in %, Vβ contribution of the β-chain to the TCR BSA in %, 1α represent the BSA contribution of the CDR1α loop as a % of the TCR BSA (same for the 2α: CDR2α, 3α: CDR3α, 1β: CDR1β, 2β: CDR2β and 3β: CDR3β). Angle represents the docking of the variable domains angle in degrees, sc represent the shape complementarity between the TCR and the pMHC-I. The average, lowest and highest values from the literature (*65*) are represented in the grey section at the bottom of the table for an easy comparison.

Table S6. D1 TCR contacts with HLA-B*35:01 presenting variants NP6, NP7 and NP10.

TCR gene	TCR residues	NP6	NP7	NP10	Bond type
		NP residues			
CDR1α	Y 37 OH	F 3, D 4N	F 3, E 4N	F 3, E 4N	HB, VdW
CDR3α	G 109	D 4	E 4	E 4	VdW
CDR3α	G 110 N	D 4 O	E 4 O	E 4 O	HB, VdW
CDR1β	V 37	V 8	I 8	V 8	VdW
CDR2β	Q 57		I 8		VdW
CDR3β	T 109 O	S 6, T 7, V 8 N	S 6, T 7, I 8 N	S 6, T 7, V 8 N	HB, VdW
CDR3β	G 110	S 6	S 6	S 6	VdW
CDR3β	G 111 O	L 5 NZ, S 6	L 5 NZ, S 6	L 5 NZ, S 6	HB, VdW
CDR3β	Q 112 O	D 4, L 5 NZ	E 4, L 5 NZ	E 4, L 5 NZ	HB, VdW
CDR3β	E 113	L 5, T 7	L 5, T 7	L 5, T 7	VdW
TCR gene	**TCR residues**	**HLA-B:35*01 residues**			**Bond type**
CDR1α	S 28			L 163	VdW
CDR1α	Y 37 O	Q 155 NE2, Y 159, L 163	Q 155 NE2, Y 159, L 163	Q 155 NE2, Y 159, L 163	HB, VdW
Fwa	F 52	R 151	R 151	R 151	VdW
Fwa	Y 55 OH	R 151, Q 155 NE2	R 151, Q 155 NE2	R 151, Q 155 NE2	HB, VdW
CDR2α	A 57	E 154, Q 155	E 154, Q 155	E 154, Q 155	VdW
CDR2α	L 58	E 154, A 158	E 154	E 154, R 157	VdW
Fwa	R 82	A 158	A 158	A 158	VdW
CDR3α	T 108 O	R 62	R 62 NH1		HB, VdW
CDR3α	G 109	R 62			VdW
CDR3α	F 111	Q 65	Q 65, T 69	Q 65, T 69	VdW
CDR1β	V 37	E 76	E 76		VdW
CDR2β	Q 57-O-NE2	T 69, Q 72-OE1, T 73-OG1	T 69, T 73-OG1	T 69, T 73-OG1	HB, VdW
CDR2β	N 58-ND2-OD1-ND2	Q 72-OE1, E 76-OE1-OE2	Q 72-OE1, E 76-OE2	Q 72-OE1, E 76-OE2	HB, VdW
CDR2β	E 63-OE1-OE2	R 75	R 75-NH1-NH2		SB, VdW
CDR2β	A 64	Q 72		Q 72	VdW
Fwb	L 66	T 69	L 68, T 69	L 68	VdW
Fwb	D 67-OD2		Q 65-NE2	Q 65	HB, VdW
CDR3β	T 109 O	L 146, A 150	L 146, A 150	L 146, A 150	VdW
CDR3β	Q 112 O	Q 155-OE1	Q 155	Q 155	VdW
CDR3β	E 113	A 150	A 150	A 150	VdW
CDR3β	T 114-OG1	R 151-NH1-NH2	R 151-NH1-NH2	R 151-NH1-NH2	HB, VdW

VdW: Van der Waals interaction (cut-off at 4 Å), HB: hydrogen bond (cut-off at 3.5 Å), SB: salt bridge (cut-off at 5 Å).

Table S7. 3180 TCR contacts with HLA-B:35*01 presenting variants NP4, NP7 and NP8.

TCR gene	TCR residues	NP4	NP7	NP8	Bond type
		NP residues			
CDR3α	D 107-OD2	L 5-NZ	L 5-NZ	L 5-NZ	HB, VdW
CDR1β	Q 29	I 8	I 8	I 8	VdW
CDR1β	T 37	I 8	I 8	I 8	VdW
CDR3β	P 108	T 7	T 7	T 7	VdW
CDR3β	T 109-OG1	L 5, S 6, T 7-OG1	L 5, S 6, T 7-OG1	L 5, A 6, T 7-OG1	HB, VdW
CDR3β	S 110-O-N-OG	L 5, S 6-N-O	L 5, S 6-N-O	L 5, A 6-N-O	HB, VdW
CDR3β	G 111	D 4	E 4	D 4	VdW
CDR3β	R 112-N-NH2-NE-O	D 4-O-OD2, L 5-NZ	E 4-O-OE2, L 5-NZ	D 4-O-OD2, L 5-NZ	HB, VdW
CDR3β	T 113-O	L 5-NZ	L 5-NZ	L 5-NZ	HB, VdW
CDR3β	D 114-OD1	L 5-NZ	L 5-NZ	L 5-NZ	HB, VdW
TCR gene	TCR residues	HLA-B:35*01 residues			Bond type
CDR1α	A 29		R 62	R 62	VdW
CDR1α	N 37	L 163	L 163	L 163	VdW
CDR1α	Y 38-OH	R 151	R 151-NH2		HB, VdW
Fwa	D 55-OD1-OD2	R 151-NH1-NH2	R 151-NH2	R 151-NH1-NH2	SB, VdW
CDR2α	R 57-NH2-NE	R 151, E 154-OE2, Q 155	R 151-NH2, E 154-OE2, Q 155	R 151, E 154-OE2, Q 155, A 158	HB, VdW
CDR2α	S 58		A 158		VdW
CDR2α	N 59-ND2	R 157, A 158, E 161-OE1	R 157, A 158, E 161	R 157, A 158, E 161-OE1	HB, VdW
CDR3α	A 110			E 58	VdW
CDR3α	G 111-O	Q 65-NE2	Q 65-NE2	Q 65-NE2	HB, VdW
CDR3α	Y 113	Q 65, I 66, T 69	Q 65, I 66, T 69	Q 65, I 66, T 69	VdW
CDR1β	Q 29-OE1	N 80-ND2	N 80-ND2	N 80-ND2	HB, VdW
CDR1β	T 37	Q 72	Q 72	Q 72	VdW
CDR2β	E 58-O-OE1	Q 72-OE1	Q 72-OE1, R 75-NH2	Q 72, R 75-NH2	HB, VdW
FWb	L 84	E 76, R 79	E 76	E 76	VdW
CDR3β	P 108	A 150	A 150	A 150	VdW
CDR3β	T 109-OG1	A 150, Q 155-NE2	A 150, Q 155-NE2	A 150, Q 155-NE2	HB, VdW
CDR3β	S 110	T 69, T 73	T 69, T 73	T 73	VdW
CDR3β	G 111	T 69	T 69	T 69	VdW
CDR3β	R 112	R 62			VdW
CDR3β	D 114-OD2	Q 155-NE2	A 150, Q 155-NE2	Q 155-NE2	HB, VdW
CDR3β	T 115-OG1	R 151-NH2	R 151-NH1-NH2	R 151-NH1	HB, VdW

VDW: Van der Waals interaction (cut-off at 4 Å), HB: hydrogen bond (cut-off at 3.5 Å), SB: salt bridge (cut-off at 5 Å).

Table S8. Healthy buffy pack donor age, sex and HLA typing.

Donor	Age (years)	Sex	HLA-A	HLA-B	Year of blood collection
d1	35	ND	01:01, 03:01	35:01, 57:01	2012
d2	66	ND	01:01, 32:01	08:01, 35:01	2013
d3	49	Male	03:01	18:01; 35:01	2016
d4	36	Male	11:01, 32:01	27:05, 35:01	2021
d5	57	Female	01:01, 03:01	18:01, 35:01	2022
d6	44	Female	02:01, 24:02	35:01, 44:02	2021
d7	30	Male	02:01, 11:01	35:01, 40:01	2021
d8	33	Male	02:01, 11:01	18:01, 35:01	2021

ND: not determined

Table S9. List of anti-human monoclonal antibodies used for flow cytometry.

Antibody	Fluorochrome	Species	Clone	Manufacturer	Catalogue #
CD3	PE	Mouse	UCHT1	eBioscience	12-0038-42
CD4	AF700	Mouse	RPA-T4	BD Pharmingen	557922
CD8α	PerCP-Cy5.5	Mouse	SK1	BD	565310
CD8α	BV650	Mouse	SK1	Biolegend	344730
CD8β	APC	Mouse	2ST8.5H7	BD Fastimmune	641058
CD14	APC-H7	Mouse	MΦP9	BD	641394
CD19	APC-Cy7	Mouse	SJ25C1	BD Pharmingen	557791
CD69	APC	Mouse	L78	BD	340560
CD107a	AF488	Mouse	eBioH4A3	eBioscience	53-1079-42
IFN-γ	V450	Mouse	B27	BD Horizon	560371
MIP-1β	PE	Mouse	D21-1351	BD Pharmigen	550078
TNF-α	AF700	Mouse	MAb11	BD Pharmingen	557996